FOG INERTING ANALYSIS
FOR PWR ICE CONDENSER PLANTS

BY

S. S. TSAI

CORE AND CONTAINMENT ANALYSIS
NUCLEAR SAFETY DEPARTMENT
WESTINGHOUSE ELECTRIC CORP.

NOVEMBER 1981

ABSTRACT

The recent hydrogen burn test conducted at the Lawrence Livermore National Laboratory has raised the NRC and the ice condenser plant owners concern about fog inerting probability and consequences in ice condenser plants. The present investigation is aimed at resolving this fog inerting issue. In this report, major fog formation and removal mechanisms that exist in the post-accident ice condenser containment are identified and quantified. Methodologies have been developed for predicting fog formation and removal rates and for predicting fog concentrations in various compartments in an ice condenser containment.

This methodology development has resulted in two computer programs, FOG and FOGMASS. The FOG computer program employs the Hijikata-Mori boundary layer fog formation theory, and calculates the fog formation rates due to boundary layer and bulk stream condensation. The computer program FOGMASS solves the mass conservation equations for fog droplets and calculates the fog concentrations in various compartments. Both computer programs have been used to predict fog concentrations in the Sequoyah, McGuire, and D. C. Cook containments, using the CLASIX output data for a S_2D accident sequence.

In order to utilize the calculational results from the study, a fog inerting criterion has been established. This criterion uses the hydrogen concentration, volume mean drop size, and fog concentration to define the fog inerting regime. For a given hydrogen concentration, the minimum fog inerting concentration was found to vary with the square of the volume mean drop size. This criterion has been verified by the Factory Mutual recent fog inerting test data.

The application of the fog inerting criterion to the three ice condenser plants shows that fog inerting would not exist in the upper and lower compartments. Fog inerting in the ice condenser upper plenum at hydrogen concentratons at which glow plug igniters are designed to operate is very unlikely.

TABLE OF CONTENTS

Section	Title	Page
	ABSTRACT	i
	TABLE OF CONTENTS	ii
	LIST OF TABLES	iv
	LIST OF FIGURES	v
1.0	BACKGROUND	1-1
2.0	INTRODUCTION	2-1
3.0	FOG GENERATING MECHANISMS IN AN ICE CONDENSER CONTAINMENT	3-1
	3.1 Fog Generated by Break Flow	3-1
	3.1.1 Amount of Fog Generated by Break Flow	3-3
	3.1.2 Drop Sizes Generated by Break Flow	3-5
	3.2 Nucleation of Fog Droplets in Containment Atmosphere	3-6
	3.2.1 Nucleation Theories	3-7
	3.2.1.1 Classical Theory of Homogeneous Nucleation	3-7
	3.2.1.2 Heterogeneous Nucleation Theory	3-9
	3.2.2 Fog Formation Conditions	3-10
	3.2.3 Conditions for Fog Formation Near a Cold Surface	3-12
	3.2.4 Rate of Fog Formation	3-15
	3.2.5 Fog Drop Sizes	3-19
	3.3 Fine Mist Droplets From Containment Sprays	3-19
4.0	FOG REMOVAL MECHANISMS IN AN ICE CONDENSER CONTAINMENT	4-1
	4.1 Settling Due to Gravity	4-1
	4.2 Agglomeration	4-2
	4.3 Vaporization	4-2
	4.4 Removal by Spray Drops	4-3
	4.5 Other Removal Mechanisms	4-3

TABLE OF CONTENTS (Continued)

Section	Title	Page
5.0	FOG INERTING CRITERIA	5-1
	5.1 Previous Work	5-1
	5.2 Present Theory	5-2
	5.3 Verification of Theories by Experiments	5-6
6.0	ASSESSMENT OF FOG INERTING PROBABILITY IN ICE CONDENSER CONTAINMENTS	6-1
	6.1 Determination of Volume Fraction of Fog Droplets in Ice Condenser Containment Subcompartments	6-1
	6.1.1 Calculation of m_{break}	6-5
	6.1.2 Calculation of m_{cond}	6-6
	6.1.3 Calculation of m_{set}	6-6
	6.1.4 Calculation of m_{sp}	6-7
	6.2 Fog Inerting Probability in the Sequoyah Plant	6-7
	6.3 Fog Inerting Probability in the McGuire Plant	6-23
	6.4 Fog Inerting Probability in the D. C. Cook Plant	6-37
	6.5 Effect of Fog on Global Combustion	6-50
7.0	SUMMARY AND CONCLUSIONS	7-1
	ACKNOWLEDGMENTS	7-3
	REFERENCES	R-1
	APPENDIX A	A-1
	APPENDIX B	B-1

0430Q:1

LIST OF TABLES

Table No.	Title	Page
6.1	FOG Input Data for Sequoyah Lower Compartment	6-18
6.2	FOG Input Data for Sequoyah Ice Condenser	6-19
6.3	Geometric Data for Sequoyah Containment	6-20
6.4	MARCH Prediction of Reactor Coolant Mass and Energy Release Rate for the S_2D Sequence	6-21
6.5	Intercompartmental Flow Rates (ft^3/sec) Predicted by CLASIX for Sequoyah	6-22
6.6	FOG Input Data for McGuire Lower Compartment	6-33
6.7	FOG Input Data for McGuire Ice Condenser	6-34
6.8	Geometric Data for McGuire Containment	6-35
6.9	Intercompartmental Flow Rates (ft^3/sec) Predicted by CLASIX for McGuire	6-36
6.10	FOG Input Data for D. C. Cook Lower Compartment	6-46
6.11	FOG Input Data for D. C. Cook Ice Condenser	6-47
6.12	Geometric Data for D. C. Cook Containment	6-48
6.13	Intercompartmental Flow Rates (ft^3/sec) Predicted by CLASIX for D. C. Cook	6-49

LIST OF FIGURES

Figure No.	Title	Page
3.1	T-S Diagram for Reactor Coolant Discharged From Break	3-4
3.2	Vapor Pressure and Temperature Profile Near a Cold Surface	3-14
3.3	Formation of Fog Near a Cold Surface	3-16
3.4	Drop Size Distribution Predicted by Neiburger and Chien	3-20
3.5	Particle Size Distribution for 50 PSI Pressure Drop Across Nozzle No. 1713	3-21
4.1	Terminal Velocity as a Function of Drop Radius in Steam-Air Atmospheres	4-5
4.2	Agglomeration Rates in Air Between Equal-Sized Drops	4-5
5.1	Minimum Ignition Energies and Quenching Distance for Hydrogen-Oxygen Inert Gas Mixtures at Atmospheric Pressure	5-3
5.2	The Effect of Droplet Spacing on Flame Quenching	5-4
5.3	Schematic Representation of Temperature Profile Through the Flame Front	5-7
5.4	The Parameter $\sqrt{\theta_i}\,\mu$ as a Function of $(Y_u - Y_f)/\theta_i$ for Different Values of $K\theta_i$	5-7

LIST OF FIGURES (Continued)

Figure No.	Title	Page
5.5	$(K)_{crit}\ e_i$ at the Flammability Limit as a Function of $(Y_u - Y_f)/e_i$	5-8
5.6	Comparison Between Theories and Factory Mutual Fog Inerting Experiments on 4.76 Percent H_2	5-10
5.7	Comparison Between the Present Theory and Factory Mutual Fog Inerting Experiments on 7.2 Percent H_2	5-11
5.8	Comparison Between the Present Theory and Factory Mutual Fog Inerting Experiments on 7.9 Percent H_2	5-12
6.1	Sequoyah CLASIX Containment Model	6-8
6.2	Fog Formation in TVA Sequoyah Lower Compartment	6-10
6.3	Fog Formation in TVA Sequoyah Ice Condenser	6-11
6.4	Fog Concentration in Sequoyah Containment	6-14
6.5	McGuire CLASIX Containment Model	6-24
6.6	Fog Formation in Duke McGuire Lower Compartment	6-25
6.7	Fog Formation in Duke McGuire Ice Condenser	6-26
6.8	Fog Concentration in McGuire Containment	6-29
6.9	D. C. Cook CLASIX Containment Model	6-38

LIST OF FIGURES (Continued)

Figure No.	Title	Page
6.10	Fog Formation in AEP Cook Lower Compartment	6-29
6.11	Fog Formation in AEP Cook Ice Condenser	6-40
6.12	Fog Concentration in D.C. Cook Containment	6-43

1.0 BACKGROUND

The incident at Three Mile Island has demonstrated that a significant amount of hydrogen could be generated during core degradation. This experience raised NRC concern about the safety of nuclear power plants, in terms of their capability to control hydrogen during severe accidents. Since ice condenser plants have a relatively small volume and low containment design pressure, the problem is magnified. Therefore, the NRC has requested the ice condenser plant owners to study hydrogen control methods for use in their plants. In this regard, the Tennessee Valley Authority (TVA), Duke Power and American Electric Power (AEP) have proposed the use of glow plug igniters at various locations inside their ice condenser containments to ignite hydrogen at low concentration.

Recently, the NRC requested Lawrence Livermore National Laboratory (LLNL) to carry out experiments on these igniters to determine their effectiveness. In these experiments, two tests with high steam concentration seemed to indicate that substantial fog formation could occur when saturated steam is discharged into a unheated vessel and under some conditions fog could effectively preclude hydrogen from combustion[1].

The LLNL tests raised some doubts about the effectiveness of glow plug igniters under fog formation conditions. In a recent review of hydrogen related issues for ice condenser plants,[2] the NRC has raised several questions concerning the probability and consequences of fog formation and steam supersaturation in ice condenser plants.

In response to the NRC questions, TVA, AEP, and Duke established experimental and theoretical analysis programs to study the fog inerting problem. The experimental program was contracted to Factory Mutual. The experiments were designed to test glow plug igniter's performance under different fogging conditions. At the same time, the plant owners requested Westinghouse to perform fog inerting analyses for the Sequoyah, McGuire, and D. C. Cook plants. This report presents the results of the Westinghouse studies.

2.0 INTRODUCTION

From the post-test analysis of the LLNL hydrogen burn tests, it appears that substantial fog formation occurred inside the test vessel. Generally, fog droplets are only few microns in diameter. These sizes of droplets have potential to prevent a flammable gas mixture from combustion or quench a propagating flame. This is because these sizes of droplets vaporize very fast (on the order of miliseconds), absorbing an enormous amount of the heat released from combustion if a substantial quantity of these droplets is present in the atmosphere. In comparison, large water droplets in the range of few hundred microns or larger (e.g. spray droplets) have no inerting effect on combustion[20] and hence have insignificant effect on glow plug igniter's performance. Therefore, the present analysis will be concentrated on the generation and removal of fog (mist), and its impact on the glow plug igniter system.

There are a number of fog generation and removal mechanisms present in a post-accident ice condenser containment atmosphere. The fog generation mechanisms include fog generated by the break flow (if it is two-phase), fog formation near the ice and structural heat sink surfaces (since the surface temperatures could be well below the dew point), and fog generation due to homogeneous and heterogeneous nucleation in condensing bulk streams.

The fog removal mechanisms include gravitational settling, agglomeration, vaporization and removal by spray droplets. In order to estimate the post-accident fog concentrations in ice condenser containments, these competing mechanisms must be studied, and evaluated. To solve this problem, it requires a numerical integration of the mass conservation equations for the mist droplets in the various containment subcompartments. By making some simplifying assumptions the transient fog concentration in the various subcompartments have been estimated.

The analysis presented here considers all the fog removal and generation mechanisms previously described. In addition, it considers the fog entrainment in the intercompartmental flows (including fan flows) in the fog mass conservation equations. In order to perform this analysis it was necessary to use CLASIX results for a S_2D event as boundary conditions to the problem.

In addition to calculation of fog concentrations in various containment compartments, it was necessary to establish a fog inerting criterion. A fog inerting criterion has been proposed by Berman et al., which predicts the minimum fog concentration required to inert a given hydrogen concentration and given volume mean fog drop size. This criterion seems to overpredict the minimum fog inerting concentration, when compared with experimental data. A more realistic fog inerting theory is presented in the present study.

The fog inerting methodology, analysis, and results are presented in the following sections of this report. Sections 3 and 4 present the methodology for calculating the fog formation and removal rates. Section 5 gives the fog inerting criteria, and Section 6 presents the results.

3.0 FOG GENERATING MECHANISMS IN AN ICE CONDENSER CONTAINMENT

The inerting capability of fog droplets depends on their sizes and concentration in the containment atmosphere, as well as the hydrogen concentration. This section is intended to identify various fog generation mechanisms present in an ice condenser containment and to determine the drop sizes and the rates of fog generation from these mechanisms. Three fog generation mechanisms are discussed in this section and the dominant fog generation mechanisms are identified.

3.1 FOG GENERATED BY BREAK FLOW

The post-LOCA containment atmosphere is most likely to be a drop-laden atmosphere. The large-scale simulated LOCA experiments conducted to date have directly or indirectly confirmed the presence of two-phase atmospheres. For example, Marvikken[3] and Battelle - Frankfurt[4] experiments were instrumented to measure fluid densities and water levels in various parts of the containment. Therefore, fog generation by the break flow cannot be neglected. The following discussion of this phenomenon pertains to small LOCAs.

In the early stage of a small LOCA transient, a substantial portion of the primary coolant discharged from the break will remain as liquid. Because of the superheat and high velocity, this liquid will be framented by aerodynamic forces and homogeneous nucleation mechanism into small droplets. These droplets are expected to be entrained by the intercompartmental and fan flows and spread to other parts of the ice condenser containment. During their travel throughout the containment, the fog droplets will be removed by gravitational settling, sprays, and vaporization. The fog generation period lasts until the water level in the reactor vessel falls to the break elevation and the break flow is no longer two-phase. For the particular S_2D sequence analyzed by

CLASIX,[5] this period lasts for about 36 minutes and about 4.2 x 10^5 lbs of water has been discharged into the lower compartment during this period of time.

After the water level in the reactor vessel falls below the break elevation, the break flow rate is substantially reduced. The flow is essentially steam and no fog droplets will be generated. As a result, the lower compartment becomes superheated afterward. Fog droplets may vaporize during their travel through this compartment and substantial removal of mist droplets are expected.

Large suspended drops generated by the break flow will be removed very quickly by gravitational settling and impingement. For the drops larger than 20 μ, the removal rate is high and complete removal only takes a few seconds. For the smallest drops (less than 1 μ) the terminal velocity is so small that they virtually remain suspended in the atmosphere indefinitely. The only effective removal mechanisms for these sizes of drops are vaporization, and collision with larger spray drops. The weight fraction of these sizes of drops is estimated to be 1 percent[3] generated by the break flow. The population of these small drops can increase if nucleation of embryos occurs in a saturated atmosphere.

3.1.1 AMOUNT OF FOG GENERATED BY BREAK FLOW

As discussed previously, the existence of a two-phase drop-laden regime has been observed experimentally. In a small LOCA, flashing of primary coolant at the break and subsequent vaporization of blowdown liquid represent a series of changes of thermodynamic states. Since the reactor coolant pressure is high, the break flow will be choked. The acceleration of primary coolant to the break location is essentially an isentropic process, in which the pressure decreases to the point at which substantial homogeneous nucleation occurs. When the flow leaves the break, the liquid is framented by both the aerodynamic forces and the nucleation mechanism into small fog droplets. These fog droplets continue to vaporize, because of the superheat in the droplets, until a thermodynamic equilibrium state is reached. Because of the high superheat and large aerodynamic forces, it is expected that the fog droplets generated are very small. This vaporization process is essentially isenthalpic.

The existence of a two phase drop-laden regime can also be explained by use of a T-S diagram for steam as shown in Figure 3.1 (Figure 1 of Reference 6). It is shown in this figure that the blowdown liquid goes through a series of thermodynamic states, starting from the subcooled liquid state B_0. The liquid expands isentropically from the subcooled state B_0 to the state B_1 at the break, where a two-phase critical flow is developed. At the same time, temperature changes from T_0 to T_1. After leaving the break, the droplets continue to vaporize because of excessive superheat until finally an equilibrium state B_2 is reached at which the droplets are in thermal equilibrium with their surroundings. This vaporization process is essentially isenthalpic. At this time, the droplet temperature drops to T_2 and the atmospheric temperature also rises to T_2. For a small LOCA, the equilibrium temperature varies with time. According to the CLASIX analysis of the Sequoyah plant, the lower compartment gas temperature rises quickly from 100°F to approximately 200°F and then stay at this temperature for an extended period of time. Using these temperatures as final equilibrium

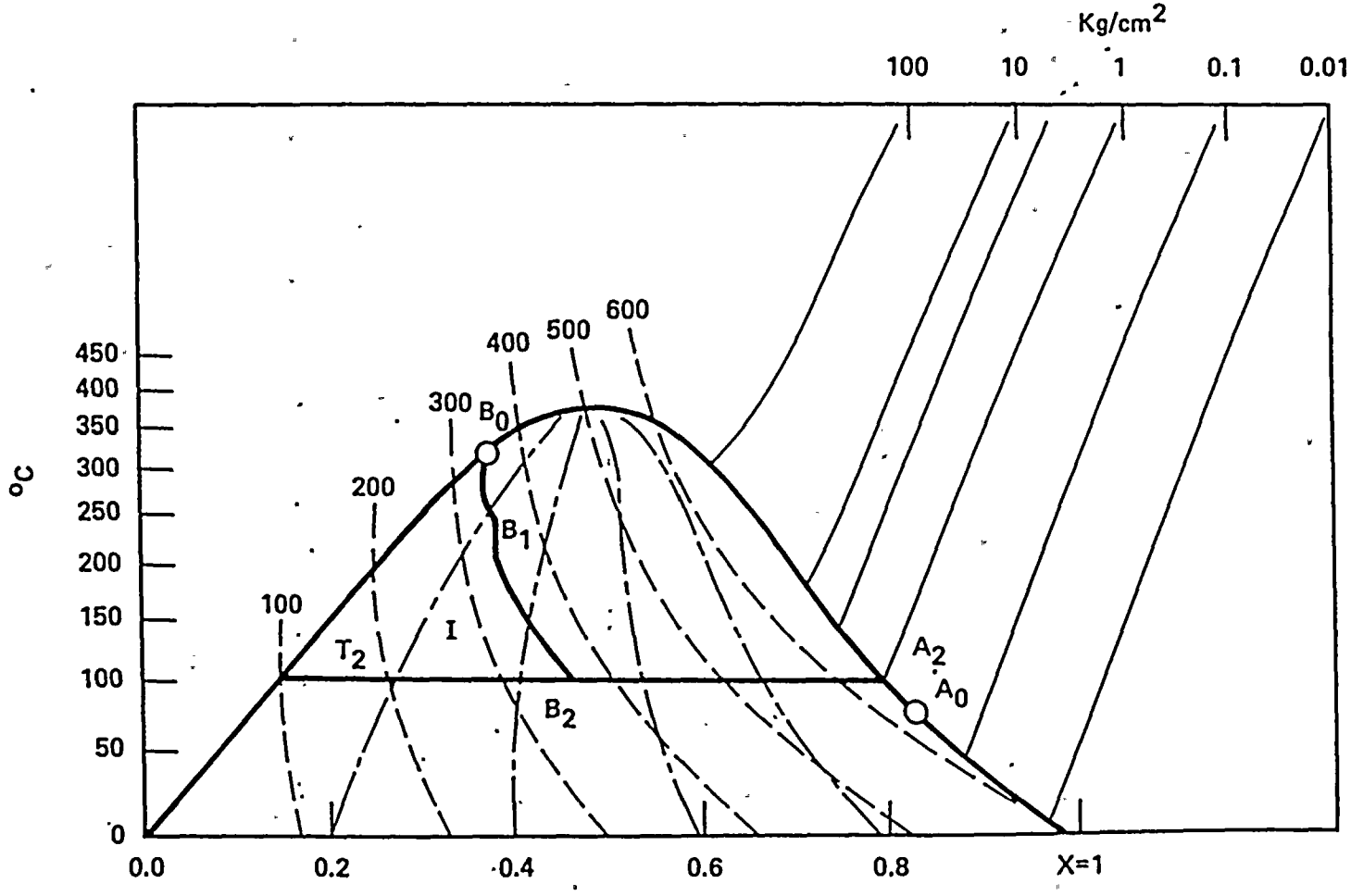

FIGURE 3.1 T-S DIAGRAM FOR REACTOR COOLANT DISCHARGED FROM BREAK

temperatures for water droplets, the weight fraction of water droplets in the break flow is approximately 50 percent, which is consistent with the MARCH calculations[7] of the break flow rate and its energy release rate.

The discussion given above is valid only when the initial state of the break flow is subcooled or saturated liquid. After the water level inside the reactor vessel falls below the break elevation, the break flow will be steam. The moisture content of the steam will be very low, even though isentropic expansion may lead to homogeneous nucleation and subsequent condensation in the vapor stream. Depending on the supersaturation that can be achieved in this isentropic expansion, a condensation shock is possible when critical supersaturation is reached. However, it is believed that the fog droplets generated by homogeneous nucleation in this supersonic jet is negligible as compared to other fog generating mechanisms. Hence, it will be neglected in this present analysis. Therefore, the fog generation by the break flow is considered possible only when the water level in the reactor vessel is above the break elevation.

According to the MARCH[7] calculation at 2172 seconds into the accident, the water level inside the reactor vessel falls below the break elevation for the S_2D case analyzed in Reference 7. By this time approximately 421,000 lbs of water has been discharged from the break and 56 percent of this discharged fluid, i.e., 236,000 lbs, will be suspended in the atmosphere as condensate. However, most of these droplets will later be removed by gravitational settling, sprays, and vaporization.

3.1.2 DROP SIZES GENERATED BY BREAK FLOW

The flashing jet experiment conducted by Brown and York[8] has indicated that the drop sizes produced by flashing liquid are small. They derived a correlation for the linear mean drop size based on the test data. The correlation shows that the mean drop size is inversely proportional to the Weber number and it decreases linearly with increasing

superheat. However, this correlation is applicable for liquid superheat less than 75°F and it can not be extrapolated to the large superheat of the reactor coolant. However, some conclusion concerning the drop sizes produced by blowdown of the reactor coolant can be drawn for this condition. The break flow has much larger superheat and Weber number than those used in this experiment; therefore, the drop sizes produced by the break flow should be much smaller than ~50μ observed in this experiment.

Gido and Koestel[9] have developed a method for estimating the drop size leaving the fragmentation/evaporation zone of a blowdown jet. This model is based on the assumption that drops with an internal temperature difference of less than 5K will escape fragmentation. This model has been verified by the low superheat data of Brown and York. Application of this method to the LOCA condition shows that the maximum attainable drop size is 7μ (this means that any drop size larger than 7μ will not escape framentation by homogeneous nucleation). The corresponding mean drop size is about 4μ, based on the observation of the largest drop size and mean drop size in the experiment reported in Reference 8. However, this volume mean drop size is not used in the present analysis. Instead, the present analysis uses 10 μ mean drop size, considering the drop agglomeration effect.

3.2 NUCLEATION OF FOG DROPLETS IN CONTAINMENT ATMOSPHERE

Nucleation of water embryos from the homogeneous vapor phase plays an important role in mist generation in ice condenser plants. Nucleation is a process by which tiny water embryos or condensation nuclei are formed from a pure vapor phase at a rapid rate. In incipient homogeneous nucleation, the local gas temperature drops below the dew point corresponding to the local steam partial pressure and some degree of local supersaturation is needed. The degree of supersaturation needed to start nucleation depends on the number of condensation nuclei present in the containment. These condensation nuclei could be very small water droplets or dust particles. If sufficient number of condensation nuclei

exist, supersaturation could be small. It is likely that the ice condenser containment contains a subtantial number of dust particles such that little supersaturation is needed for nucleation.

This section is devoted to the discussion of fog formation by homogeneous or heterogeneous nucleation. The classical nucleation theories are used to explain the nucleation phenomenon.

3.2.1 NUCLEATION THEORIES

The process of nucleation of an embryo water drop is important in understanding the mechanism of fog formation in ice condenser plants. Two types of nucleation process, namely, homogeneous and heterogeneous nucleations, and their theories will be discussed in Section 3.2.1.

3.2.1.1 CLASSICAL THEORY OF HOMOGENEOUS NUCLEATION

When an embryo droplet, usually assumed spherical, is formed from condensation of water vapor molecules, its free energy changes. The change of free energy can be expressed as

$$\Delta G = 4\pi r^2 \sigma - (4/3)\, \pi r^3 n_L KT \ln (P/P_0) \qquad (3.1)$$

where σ is the surface free energy per unit area, or surface tension, r is the drop radius, P is the vapor pressure, P_0 is the saturation pressure at the droplet temperature, n_L is number of molecules per unit volume, K is the Boltzman constant, and T is the drop temperature. The supersaturation S, is defined as P/P_0.

Equation (3.1) represents a free energy barrier to the growth of the drops at a given suprsaturation. At maximum ΔG, the critical radius r* can be obtained from Equation 3.1 as

$$r^* = \frac{2\sigma}{n_L KT \ln (P/P_0)} \qquad (3.2)$$

The drops of the critical size can be considered as condensation nuclei since at this size the drops will grow with no change in free energy. This critical size represents an equilibrium size at which a supersaturated vapor at vapor pressure P is in equilibrium with this critical drop at a lower saturation pressure P_0. However, this equilibrium mode is unstable. For example, if a drop of the critical size originally in equilibrium with the surrounding vapor suffers a sudden small increase in size due to condensation, then (if the drop temperature does not change), Equation 3.2 shows that the equilibrium pressure, P, on its surface will decrease. Therefore, the actual vapor pressure will then be greater than the equilibrium value and further condensation will occur. This is why the drop of this critical size is called condensation nucleus.

The nucleation rate of critical-sized embryos can be obtained from the kinetics of a nonequilibrium distribution of embryos. The classical nucleation theory[10] shows that there is a very sudden increase in the nucleation rate when past a certain critical value of supersaturation. An extensive validation of the nucleation theory was conducted by Volmer and Flood[11] in an experiment in which a number of vapors were expanded to visible condensation in a cylinder. The observed critical supersaturations agreed suprisingly well with theory in nearly all cases, including water vapor.

Critical condensation nuclei sizes typically range from 10 to 100 atoms. These sizes are considerably smaller than the mean free path of the vapor molecules and therefore the rates of mass and heat transfer at the drop surface cannot be predicted by bulk transport theories. In this case, the kinetic theory of gas should be used to predict the rates of mass and heat transfer at the drop surface.

Starting from the kinetic theory of gas and the energy conservation equation, the rate of growth of a condensation nucleus was obtained by Hill et al.[10] It was found that the growth rate is on the order of 10^{-3} ft/sec. Therefore, it takes only about 1 millisecond for the condensation nucleus to grow to a fog droplet size of 1 μ.

3.2.1.2 HETEROGENEOUS NUCLEATION THEORY

Another mechanism of forming embryos is heterogeneous nucleation on foreign particles that could suspend in the containment atmosphere. These particles may serve as nucleation sites for vapor and thus enhance the nucleation rate. The source of foreign particles in the containment following core degradation could come from fission product aerosols and dust particles. The size distribution of these particles are important because the supersaturation required to form embryos depends on particle sizes.

A typical size distribution of atmospheric aerosols is that of Junge[12], taken from surveys made near Frankfurt A.M., Germany. The surveys found that the size range of dust particles is from 0.01 to 1 μ. In the range from 0.01 to 0.5 μ, there are between 100 and 10,000 particles per cubic centimeter. A majority of particles have sizes smaller than 1 micron. At the smallest size of 0.01 μ, the critical supersaturation is about 1.02 and at the largest size the supersaturation is only 1.001.

The other source of aerosol particulates is fission products. During normal operation, the primary coolant contains very little fission products. However, a large release of fission products, such as the gap release, could occur at about the same time the hydrogen releases. The amount of fission products released to the containment depends on accident scenarios. The distribution and transport of fission products in the containment can be predicted by the CORRAL code[13]. The size distribution of fission products in the containment can be extrapolated from the CSE experiments[14]. These experiments indicated that soon after fission product release, the mean particle diameter was 15 μ. A few hours later, the mean diameter decreased to about 5 μ because of settling of large particles onto the floor. These sizes are substantially larger than those of dust particles and therefore, critical supersaturation is even smaller than values quoted above for the dust particles.

The atmospheric aerosols consist of particulates of various sizes, various chemical components, and various electrostatic charges. The aerosol particulates could be soluble or insoluble in water. All these properties could affect the required supersaturation for nucleation.

In the case of insoluble particulates, the contact angle, ϕ, between the embryo and the particle surface is important. If the particle is completely wettable, $\phi = 0$, it forms a base on which a small amount of water can form a drop of large radius of curvature and thus satisfy the Hemholtz equation (Eq. 3.2) at a much lower supersaturation than would be the case if same number of molecules form a drop with a particle core. Fletcher[15] developed a relationship between the supersaturation and drop radius for several values of contact angle, assuming that the particle is spherical. Competely wettable, a particle of 1 micron or so, when covered with a film of water, is theoretically at the critical radius, and it needs only 1.001 critical supersaturation.

The post-accident containment atmosphere is likely to contain a substantial amount of aerosol particles. These particles will act as condensation nuclei and therefore, little supersaturation is required to precipitate condensation.

3.2.2 FOG FORMATION CONDITIONS

Fog formation in a mixture of vapor and noncondensible gases has been of interest to meteorologists, and turbine and condenser designers. Fog is formed by homogeneous or heterogeneous nucleation as a result of temperature drop below the dew point (sometimes with concommitant pressure drop). During the temperature drop, a local gas element will go through a series of thermodynamic states. Eventually, a state is reached at which incipient fog formation occurs. Some degree of vapor supersaturation is needed to precipitate fog formation. The vapor supersaturation at which rapid nucleation of vapor first appears is called critical supersaturation. The critical supersaturation, in general, is a

function of temperature, vapor properties, mixing time (if a mixing process is involved), and concentration and sizes of foreign particles. The critical supersaturation data for water has been given in Reference 15.

Fog formation in an ice condenser containment as a result of homogeneous or heterogeneous nucleation could occur: (i) inside the thermal boundary layer near a cold surface, (ii) in adiabatic or nearly adiabatic expansion of vapor jet, and (iii) in mixing of a hot vapor stream with another cooler gas.

Surface cooling may create a region of local supersaturation within the thermal boundary layer, even though the bulk stream is still superheated. If the local supersaturation reaches the critical supersaturation, incipient fog formation will commence. This condensation mechanism may exist in any compartments within the containment especially in the ice condenser where ice temperature is well below the dew point.

When a high speed vapor - noncondensible gas mixture jet goes through an adiabatic or nearly adiabatic expansion, the gas mixture temperature and pressure will drop rapidly such that condensation may occur somewhere in the expansion process. This is the case when a hydrogen-steam mixture jet exits from a break at a supersonic speed. The jet experiences a rapid expansion and if critical supersaturation is reached, condensation shock may occur somewhere within the expanding jet. This condensation mechanism can only occur in a compartment in which the hydrogen-steam mixture jet exists.

Condensation in a fast expanding vapor - noncondensible gas jet is a localized phenomenon. Usually very little moisture is generated in the expansion process even if a condensation shock does exist. Therefore, the present study does not attempt to treat the condensation shock as a source of fog formation.

The third mechanism, condensation due to mixing, may exist in a compartment where a hot hydrogen-steam mixture mixes with a relatively cold containment atmosphere. During the mixing process, local critical supersaturation within the mixing gas could be reached and condensation would ensue. This mechanism could exist in the lower compartment in which relatively cold gas from the upper compartment is returned by the deck fans and mixed with the hot humid air.

Thus, the mixing of cold and hot vapor streams will be treated in the present study. However, only bulk condensation is considered. That is, it is not intended to compute the temperature profile to predict the local condensation rate. Instead, the bulk gas is assumed at one uniform temperature, and bulk condensation will occur when mixing results in saturation conditions. This is consistent with the CLASIX code assumption of uniform gas temperature.

Because of time restriction, it is almost impossible to treat all the condensation mechanisms. However, major condensation mechanisms will be identified and treated in the present study.

Before entering into the discussion of the methodology to calculate the fog formation rates from various fog formation mechanisms, a discussion of fog formation conditions is necessary. Since the bulk condensation approach for the mixing process has been adopted, the fog formation conditions for the mixing process are simply that critical supersaturation is reached in the bulk stream. For practical purposes, the critical supersaturation is assumed to be one since it is likely that plenty of condensation nuclei exist in the atmosphere before mixing condensation takes place.

3.2.3 CONDITIONS FOR FOG FORMATION NEAR A COLD SURFACE

Fog starts to form at a fast rate near a cold surface when local vapor supersaturation reaches the critical supersaturation. Near the cold surface, a thermal boundary layer is formed, within which local vapor pressure and saturation pressure vary. Typical vapor pressure and

temperature profiles, when the incipient homogenous nucleation first appears, are shown in Figure 3.2. It is seen in this figure that when the local vapor pressure reaches the critical vapor pressure there is a sudden appearance of fog in the boundary layer due to the fast nucleation rate. Rosner and Epstein[11] have derived fog formation conditions near a cold surface, assuming that the local vapor pressure curve is tangent to the critical vapor pressure curve at the fog incipient point. A more general fog formation criterion was given by Hijikata and Mori[17] is

$$\frac{\Delta W}{\Delta T} > \left(\frac{dW}{dT}\right)_{wall} \tag{3.3}$$

where $\Delta W = W - W_w$

$\Delta T = T - T_w$

and the weight fraction of condensing vapor, W, can be related to the partial pressure of the condensing vapor P_v as

$$W = \frac{(P_v/p)\,(M_v/M_g)}{1 - (P_v/p)\,(1 - M_v/M_g)} \tag{3.4}$$

where P = total pressure

M_v = vapor molecular weight

M_g = noncondensible gas molecular weight

Equation (3.3) may be rewritten as

$$n > 2 \tag{3.5}$$

where

$$n \equiv 2 \frac{\Delta W}{\Delta T} / \left(\frac{dW}{dT}\right)_{wall}$$

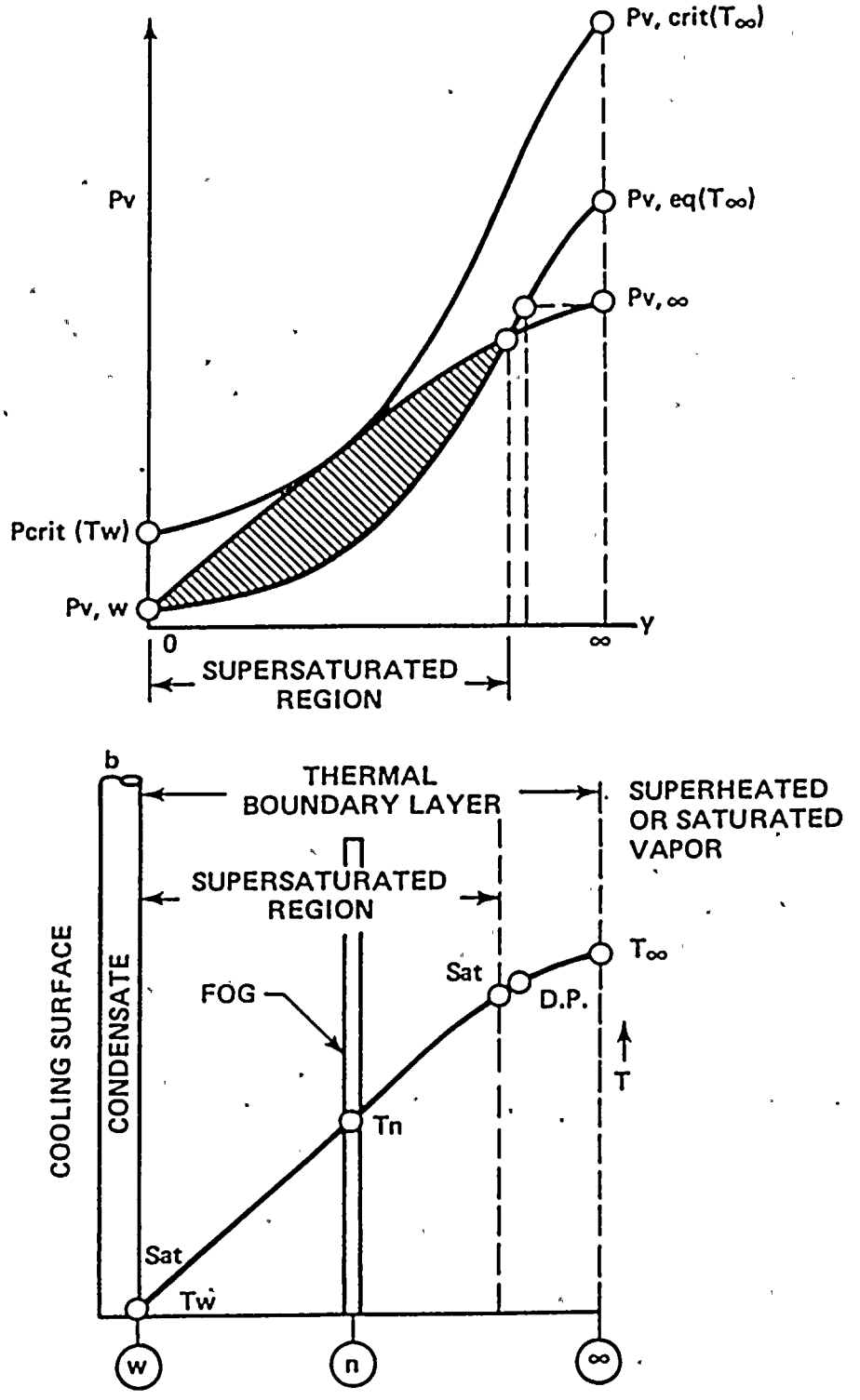

FIGURE 3.2 VAPOR PRESSURE AND TEMPERATURE PROFILES NEAR A COLD SURFACE

The parameter n is used in the following section to calculate the fog formation rate. It will be demonstrated that when $n < 2$, no fog formation is possible.

3.2.4 RATE OF FOG FORMATION NEAR A COLD-SURFACE

As has been discussed in Section 3.2.3, fog will form near cold surfaces (e.g., in the ice condenser early in the transient.) As discussed in Section 3.2.1, once water embryos are formed it takes only a few miliseconds for them to grow to the micron size. After these micron size fog droplets are formed, it needs very little supersaturation for further growth. Therefore, in the present analysis, it is assumed that vapor and droplets are in thermal equilibrium and local vapor pressure is equal to the local saturation pressure. This section is concerned with the transport of these micron-size fog droplets within the thermal boundary layer.

The boundary layer fog formation rate can be determined using the Hijikata-Mori theory[17] of fog formation in the thermal boundary layer. It was assumed that a thin liquid film, having a thickness of δ_ℓ on a cold surface, coexists with a gas-droplet flow in a two-phase boundary layer of thickness δ outside the liquid film as shown in Figure 3.3.

It was further assumed that the saturation condition exists within the two-phase boundary layer and the boundary layer approximation is applicable. Numerical solutions were obtained for the mass fraction of fog droplets, Y_o, at the gas-liquid film interface. The fog droplet flow rate at a distance X along the plate may be expressed in terms of Y as

$$\dot{m}_f = L \rho \int_0^\delta Yudy \qquad (3.6)$$

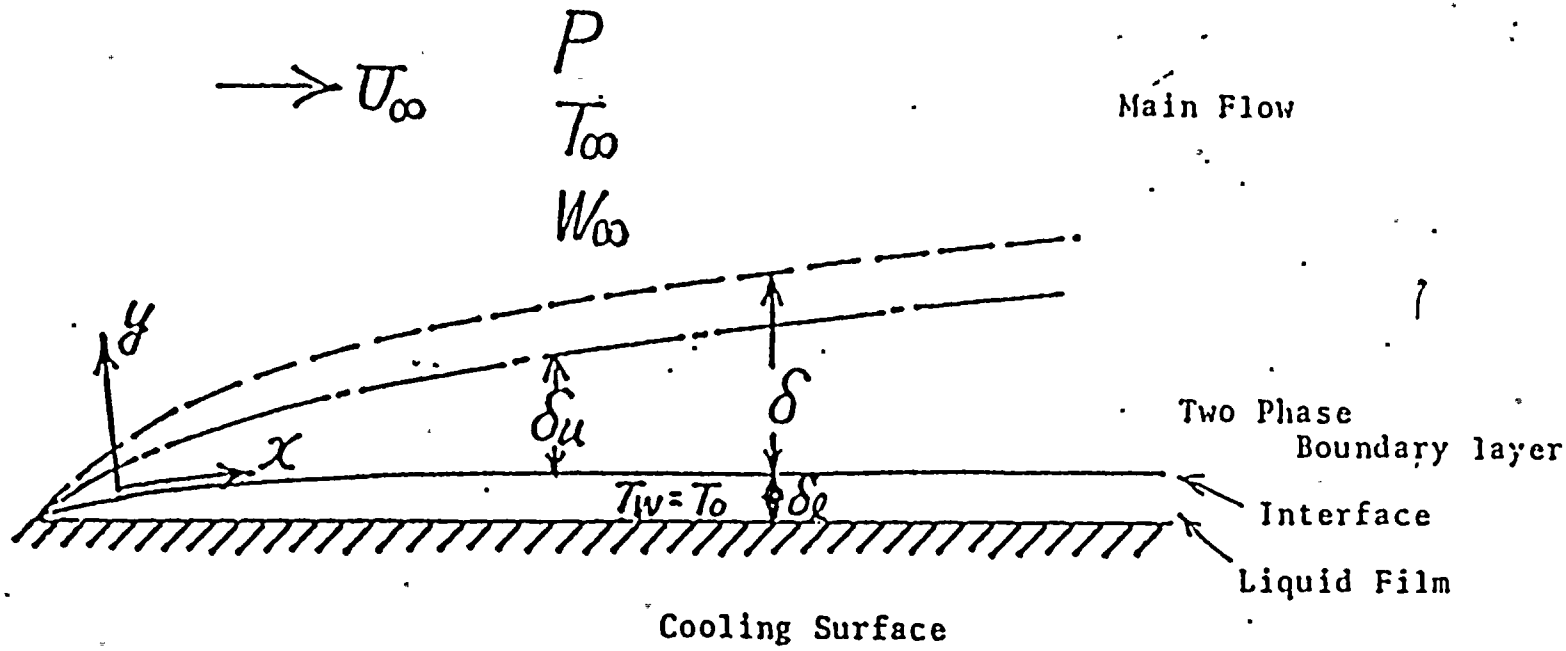

FIGURE 3.3 FORMATION OF FOG NEAR A COLD SURFACE

where Y = mass fraction of fog droplets in the boundary layer

ρ_ℓ = fog droplet density

ρ_v = vapor density

ρ_g = noncondensible gas density

Y_o = $\rho_\ell|_{y=o}/(\rho_v + \rho_g)$

y = coordinate perpendicular to the plate

δ = fog boundary layer thickness

L = width of boundary layer

ρ = $\rho_v + \rho_g$

Using the boundary layer approximations

$$Y = Y_0 (1 - y/\delta) \tag{3.7}$$

$$u = U_\infty \left\{\frac{3}{2} \left(\frac{y}{\delta_u}\right) - \frac{1}{2} \left(\frac{y}{\delta_u}\right)^3\right\} \tag{3.8}$$

$$\delta (x) = a\, x^{1/2} \tag{3.9}$$

$$\delta_u = \delta (x) (1 - \xi) \tag{3.10}$$

where a = known constant

ξ = known constant

U_∞ = free stream velocity

Substituting Eqs. (3.7) through (3.10) into Eq. (3.6), we have the rate of fog formation

$$\dot{m}_f = \rho L \delta Y_o U_\infty \left\{ \frac{0.25}{1 - \xi} - \frac{0.025}{(1 - \xi)^3} \right\} \tag{3.11}$$

Derivation of expressions for a, Y_o, and ξ is given in Appendix A. Even though boundary layer fog formation may occur in any containment subcompartment, the fog formation rate is likely to be small except in the ice condenser. For fog formation in the ice condenser, L is the total length of the periphery and x is the height of the ice bed.

During fog formation in the boundary layer, heat transfer to the cold surface will decrease the bulk fluid temperature. If the bulk fluid temperature drops below the dew point corresponding to the free stream vapor pressure, then bulk stream condensation could occur. In this case, it is assumed that the boundary layer thickness, δ, will grow so thick that $L\delta U_\infty$ becomes the gas volumetric flow rate Q through the condensing compartment. This is a very conservative assumption in terms of the fog formation rate. Under this assumption Equation (3.11) becomes

$$\dot{m}_{cond} = \rho Q Y_o \left\{ \frac{0.25}{1 - \xi} - \frac{0.025}{(1 - \xi)^3} \right\} \tag{3.12}$$

where $\dot{m}_{cond}$ is the sum of boundary and bulk stream fog formation rates.

3.2.5 FOG DROP SIZES

As mentioned earlier, when homogeneous nucleation commences, a large number of condensation nuclei are formed and they grow to the micron size within a few milliseconds. In heterogeneous nucleation, fog droplets grow on aerosal particles, which are usually less than 1 μ. In any case, the final drop sizes are determined by the atmospheric conditions with which the drops are in thermal equilibrium.

Neiburger and Chien[18] studied the growth of cloud drops by condensation and calculated droplet size distribution based on a cloud cooling rate of 6°c/hr. The initial size distribution of condensation nuclei (sodium chloride) were chosen to correspond to available observations as shown in Figure 3.4 (designated as 0 second). The calculated drop size distributions at 3000 and 6000 seconds are shown in Figure 3.4. It is seen that the sizes of fog droplets range from 0.01 μ to 20 μ. The volume mean drop size is 8 μ at 3000 second. The volume mean drop size for homogeneous nucleation is expected to be smaller than this value. Fogs of volume mean drop sizes ranging from 9 to 14 μ[30] have been observed to exist in a natural enviroment, e.g. valley. In the present study, a volume mean fog drop size of 10 μ is chosen for fog deposition and inerting calculations.

3.3 FINE MIST DROPLETS FROM CONTAINMENT SPRAYS

The containment sprays produce fairly large drop sizes. A typical containment spray nozzle, e.g., Spraco 1713 nozzle, produces the size distribution as shown in Figure 3.5, using a pressure difference of 50 psi across the nozzle[19]. It is seen that water droplets produced from containment range from 100 μ to 2000 μ. These large drops have little effect on hydrogen combustion and flammability limits, as already demonstrated in the Fenwal tests[20] and more recent tests at Factory Mutual[21]. To affect the combustion characteristics of a hydrogen mixture, the drop sizes have to be smaller than about 20 μ, namely in the fog drop size ranges. Since containment sprays essentially do not produce drops in this size range, containment sprays will not be considered as a means to produce fog droplets. Rather, it will be considered as a means to remove the fog droplets.

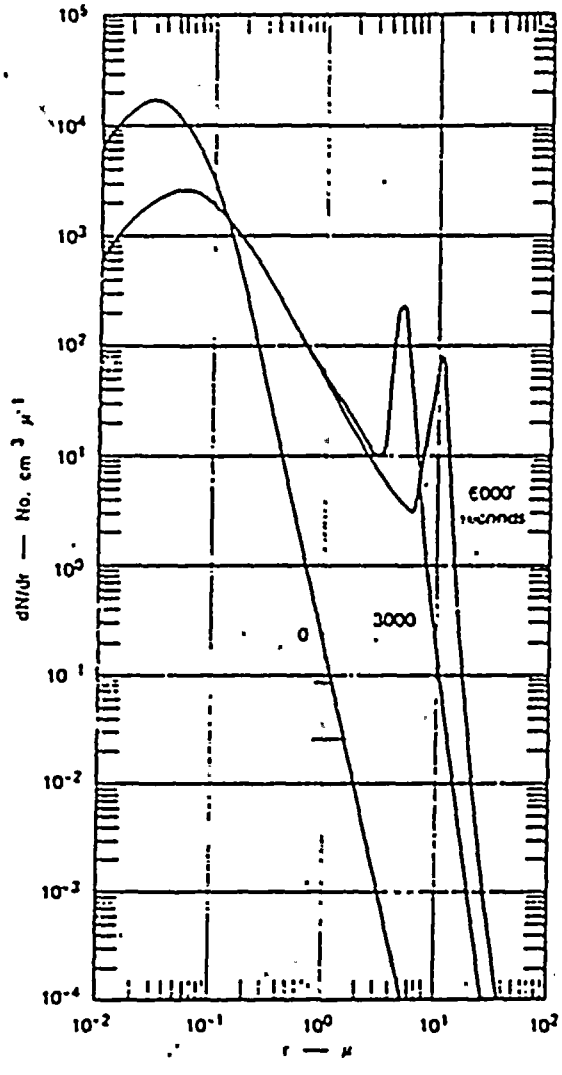

FIGURE 3.4 CLOUD DROP SIZE DISTRIBUTION PREDICTED BY NEIBURGER AND CHIEN

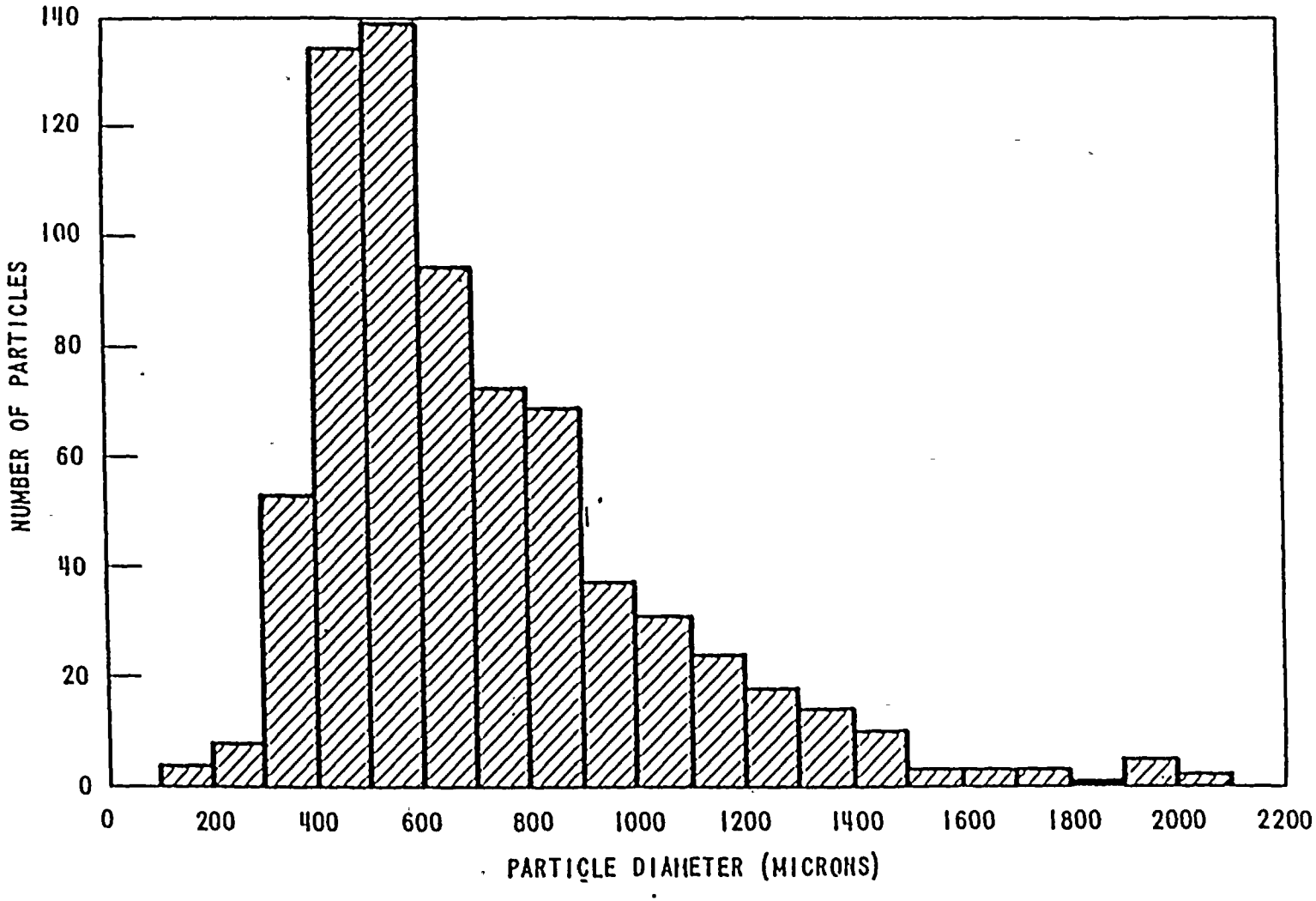

FIGURE 3.5 PARTICLE SIZE DISTRIBUTION FOR 50 PSI PRESSURE DROP ACROSS NOZZLE NO. 1713

4.0 FOG REMOVAL MECHANISMS IN AN ICE CONDENSER CONTAINMENT

In Section 3, the mechanisms of generating fog droplets were discussed. After these droplets are generated, they can be removed from the containment atmosphere by gravitational settling, vaporization, containment sprays, and impingement on structures. They can also coalesce with other drops during collision and form bigger drops. These bigger drops could easily settle out of the atmosphere under gravity. These fog droplet removal mechanisms will be discussed in this section.

4.1 SETTLING DUE TO GRAVITY

Drop removal rates due to gravitational settling depend strongly on drop radius. The removal rate increases linearly with drop terminal velocity, drop concentration, and settling area. The relationship may be expressed as

$$\dot{m}_{set} = V_t \, \eta \, A \qquad (4.1)$$

where η is the mass of mist droplets per unit volume, and A is the settling area.

The terminal velocity, V_t, is a strong function of drop radius and the relationship is shown in Figure 4.1. It is seen that the terminal velocity is approximately a linear function of drop radius in both laminar the turbulent regimes. For a 1000 μ drop, its terminal velocity is above 1 m/s, while for a 10 μ drop, which is the typical fog drop size, its terminal velocity is only about 1 cm/s. Therefore, there is very little removal by gravity for fog droplets.

4.2 AGGLOMERATION

After the fog droplets are produced, the droplets will undergo changes in the number density and size distribution with time, when drops collide with each other and coalesce. The agglomeration rate (No. of particle per unit volume per unit time) has been found to be proportional to the square of the drop population density and the coagulation mechanisms dependent rate constant K[22].

For drops larger than 1 μ, the dominant mechanism is the difference in velocities between drops in adjacent streamlines. This is usually termed the velocity gradient coagulation. For drops smaller than 1 μ, the velocity gradient effect becomes small, and drops are brought together by Brownian motion. This leads to greatly different agglomeration rates for different initial drop sizes. A typical agglomeration rate as a function of drop size in a moderately turbulent atmosphere is shown in Figure 4.2. In Figure 4.2, the sharp rise of the agglomeration rate with drop diameter larger than 1 μ implies that the larger drops agglomerate quickly to the maximum stable size supported by the atmospheric turbulence. The agglomeration rates for drops less than 1 μ are very small. Since most of the fog droplets are in micron size ranges, the agglomeration rate is not large. It is assumed in the present analysis that the initial 4 μ blowdown mean drop size will grow to 10 μ (See Section 3.2.5). Agglomeration as a separate mechanism for fog growth has been conservatively neglected.

4.3 VAPORIZATION

Fog droplets suspended in the containment atmosphere is considered to be in thermodynamic equilibrium with the surrounding gas. When the surrounding atmosphere becomes superheated or when the droplets are entrained into a superheated subcompartment, it can undergo vaporization or condensation.

In the present analysis, it is assumed that water vapor and mist droplets are in thermal equilibrium at all times. Therefore, the amount of vaporization or condensation will be determined by the thermal equilibrium state reached by the vapor and drops. In other words, it is not intended to model heat transfer between the drops and the surrounding gas, and thus determine the vaporization rate. This is a good assumption for the small fog drop sizes.

4.4 REMOVAL BY SPRAY DROPS

As mentioned above, the containment spray droplets range from 100 μ - 2000 μ, which are substantially larger than the fog droplets. If fog droplets enter the spray zone, they will probably be removed by the spray droplets by colliding with them, since the spray drop mass is much larger than the fog drop mass. A simple analytical model is used in the present study which assumes that all the fog droplets residing in the spray zone will be swept by the sprays to the floor with the spray drop removal efficiency E. The spray removal rate may be expressed as

$$\dot{m}_{sp} = E\, Q_{sp}\, M_c / n_{sp}\, V \qquad (4.2)$$

where E = spray drop removal efficiency

Q_{sp} = volumetric flow rate of sprays

n_{sp} = volume fraction of spray droplets in the spray zone

M_c = mass of fog in compartment volume V

4.5 OTHER REMOVAL MECHANISMS

Another similar mechanism for fog removal is the formation of droplets in the ice condenser. These droplets which would be generated in the ice bed when the ice melts, would fall through the ice bed, and remove fog droplets from the flow through the ice condenser. This large quantity of water would be effective in removing fog droplets. However, due to difficulty in modeling this removal mechanism, it is conservatively neglected in the present analysis.

In addition to the removal mechanisms mentioned above, fog can also be removed by impacting structural surfaces. Due to the inertia of fog droplets, substantial fog removal by impacting structural surfaces could occur, when the drop-laden mixture flow passes through long, narrow, curved paths, such as ice basket flow paths, and fan ducts. Moreover, the centrifugal force exerting on the fog droplets, when they pass through the fans, could cause the fog droplets to impact the blade surfaces or other parts of the fans. These removal mechanisms are believed to be significant; however, they are conservatively neglected in the present analysis. It is, therefore, believed that the present analysis is very conservative.

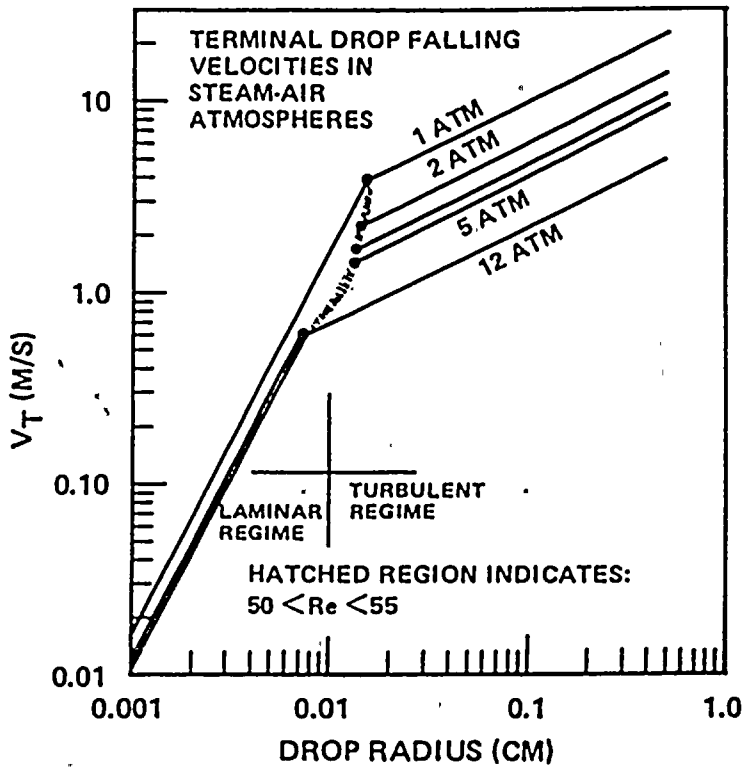

FIGURE 4.1 TERMINAL VELOCITY AS A FUNCTION OF DROP RADIUS IN STEAM-AIR ATMOSPHERE

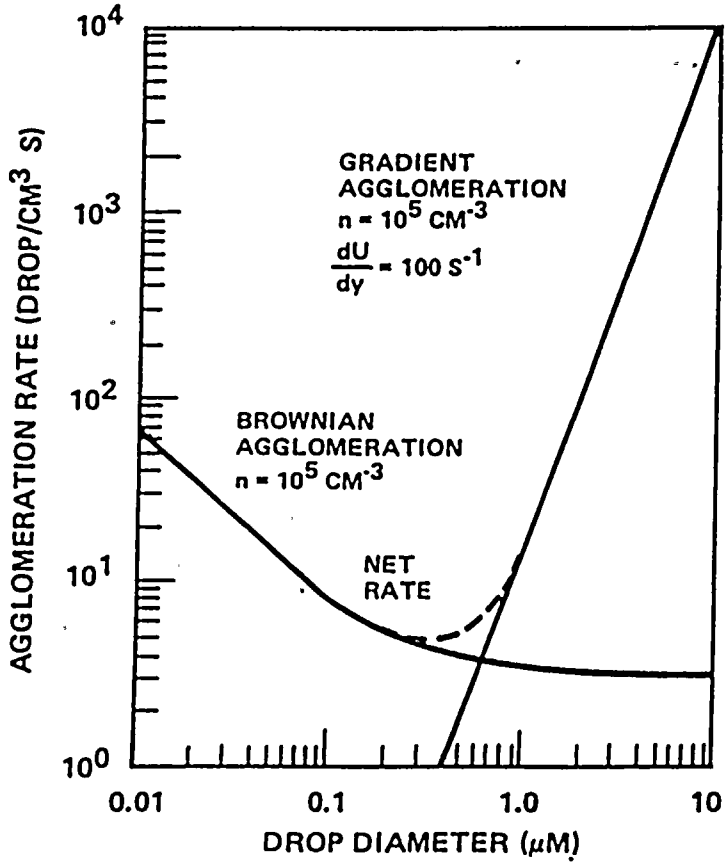

FIGURE 4.2 AGGLOMERATION RATES IN AIR BETWEEN EQUAL-SIZED DROPS

5.0 FOG INERTING CRITERIA

Recent hydrogen burn experiments conducted at Lawrence Livermore Laboratory indicated that substantial fog formation could occur when saturated steam is discharged into an unheated vessel. It appeared that this fog prevented a glow plug igniter from successfully igniting the hydrogen mixture in the vessel. The ability of fog in inhibiting and quenching of hydrogen combustion can be explained as follows. The fog droplets suspended in the hydrogen-air-steam mixture act as a heat sink that could absorb a large amount of combustion heat, greatly reducing the pressure and temperature rises resulting from hydrogen combustion. If droplets are sufficiently small such that they could vaporize inside the thin (1mm) flame front, the flame may be quenched or inhibited. For a flame speed of 2 m/s, the drop residence time is of the order of 0.5×10^{-3} seconds.[24] In such a short period of time, the droplets of initial radius less than about 4 μ will vaporize entirely in the flame front.

The quenching of a propagating flame is also governed by the distance between droplets. As the droplets become closely packed, the total droplet surface area available for energy loss increases. A critical spacing between droplets exists such that a large fraction of the heat released is absorbed, thus preventing flame propagation. This critical spacing is known as the "quenching distance", which is usually determined by propagating flames in tubes.

5.1 PREVIOUS WORK

The effectiveness of fog droplets in inhibiting or quenching a flame depends on its quenching distance, was determined by Berman et al.[24] as

$$d_q = [4V/S]_{crit} \qquad (5.1)$$

where V is the gas volume and S is the heat transfer surface area. For a hydrogen-air mixture, the data on the quenching distance is shown in

Figure 5.1. In the suspended fog droplets, this volume-to-surface ratio (i.e., V/S) is equal to

$$\frac{1}{6} \frac{d\,(1 - \eta)}{\eta}$$

where d is the mean droplet diameter and η is the volume fraction of water. When four times this ratio approaches the quenching distance, a critical droplet diameter can be obtained as

$$d_c = \frac{3}{2} \frac{\eta d_q}{1 - \eta} \qquad (5.2)$$

Using this criterion for quenching a flame, for a given volume fraction of water and gas composition, d_q can be determined. The critical droplet diameter then can be determined from the above equation. The drop sizes less than the critical drop size is capable of quenching a flame.

A plot of Eq. (5.2) for two hydrogen concentrations is shown in Figure 5.2.

5.2 PRESENT THEORY

The previous theories do not model the heat transfer and combustion processes occurring between the burned gas and the suspended droplets. A new theory has been developed, which models the heat loss and combustion.

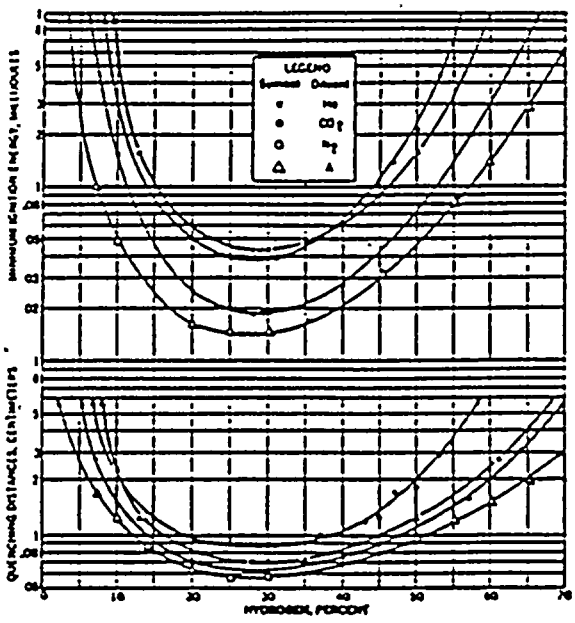

FIG. 5.1 MINIMUM IGNITION ENERGIES AND QUENCHING DISTANCE FOR HYDROGEN-OXYGEN INERT GAS MIXTURES AT ATMOSPHERIC PRESSURE

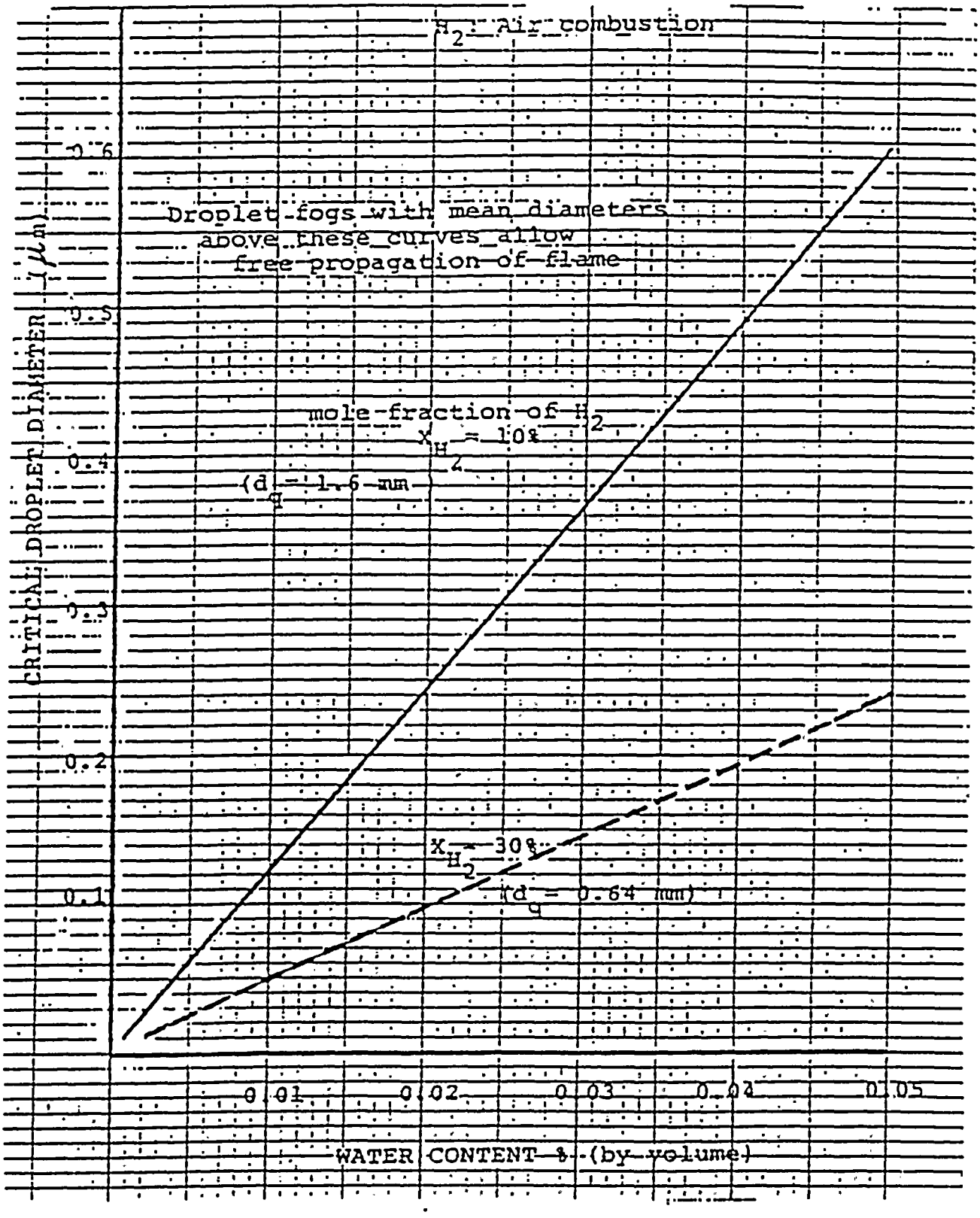

FIGURE 5.2 THE EFFECT OF DROPLET SPACING ON FLAME QUENCHING

Consider a hydrogen/air/steam/mist droplets mixture in which a flame is propagating. The flame may be divided into three zones: heating zone, reaction zone, and post-reaction zone as shown in Figure 5.3. The unburned gas at temperature T_u move in the reacton zone with the laminar burning velocity S_u. If the unburned gas density is ρ_u, then the constant mass flow rate m is equal to $\rho_u S_u$. The unburned gas is heated to ignition temperature T_i and burned in the reaction zone to reach the flame temperature T_f. The fog droplets will act as a heat sink that reduces the flame temperature. The problem has been formulated and solved by von Karman[25]. In his formulation, three energy equations, which incorporate the heat loss terms, were written for the three zones described above. The solution to these equations yields the following relationship

$$2\,K\theta_i = \left\{1 - \exp\left(-\frac{1}{2}\mu^2\right)(Y_u - Y_f)\left[1 + \sqrt{1 + (4\,K/\mu)^2}\right]\right\} \times \left\{1 - \frac{1}{\sqrt{1 + K/\mu^2}}\right\} \qquad (5.3)$$

where $\theta_i = \bar{C}_p\,(T_i - T_u)/q$

$\mu = \sqrt{\bar{C}_p / \bar{\lambda}w}\; m$

$K\theta_i = (S/\bar{C}_p w)\,\theta_i$

= the ratio of heat loss rate per unit volume to the heat release rate by chemical reaction per unit volume

q = heat of combustion

$\bar{C}_p$ = mean specific heat

$\bar{\lambda}$ = heat conductivity

w = reaction rate (mass of fuel consumed per unit time per unit volume)

Y_u = hydrogen mass fraction in the heating zone

Y_f = hydrogen mass fraction in the reaction zone

m = $\rho_u S_u$

A plot of Eq. (5.3) is shown in Figure 5.4. It is seen that for a given $K\theta_i$, there is a minimum value of $(Y_u - Y_f)/\theta_i$. Below this minimum value, there is no solution for the $\sqrt{\theta_i}\ \mu$. Therefore, this value is considered as the flammability limit. At the flammability limit, the value of $K\theta_i$ can be determined from Figure 5.4 or from Eq. (5.3) as

$$(K)_{crit}\ \theta_i = f\ ((Y_u - Y_f)/\theta_i) \tag{5.4}$$

A plot of $(K)_{crit}\ \theta_i$ as a function of $(Y_u - Y_f)/\theta_i$ is shown in Figure 5.5. Equation (5.4) may be expressed as

$$\frac{n}{d^2} = \frac{q\ \bar{C}_p\ \rho_u^2\ Su^2\ (Y_u - Y_f)\ f\left(\frac{Y_u - Y_f}{\theta_i}\right)}{12\ \bar{\lambda}^2 (T_i - T_u)} \tag{5.5}$$

Detailed derivation procedure for Eq. (5.5), is given in Appendix B. Using the data on S_u from Reference (26) we can calculate the right hand side of Eq. (5.5) for a given composition and initial gas temperature.

5.3 VERIFICATION OF THEORIES BY EXPERIMENTS

Experiments have been conducted at Factory Mutual to study the effects of water fog density, droplet diameter, and temperature on the lower

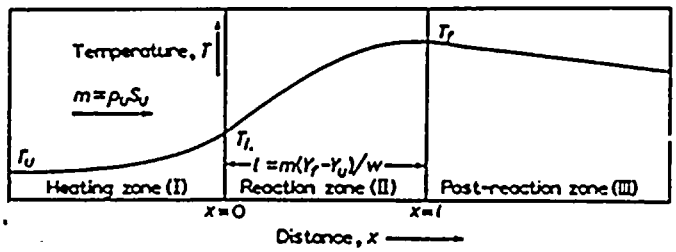

FIGURE 5.3 SCHEMATIC REPRESENTATION OF TEMPERATURE PROFILE THROUGH THE FLAME FRONT

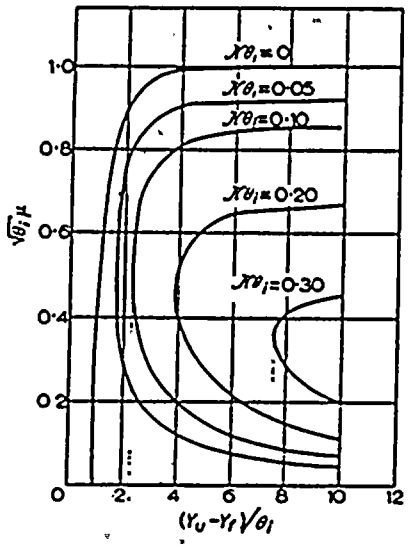

FIGURE 5.4 THE PARAMETER $\sqrt{\theta_i}\ \mu$ AS A FUNCTION OF $(Y_u - Y_p)/\theta_i$ FOR DIFFERENT VALUES OF $K\theta_i$

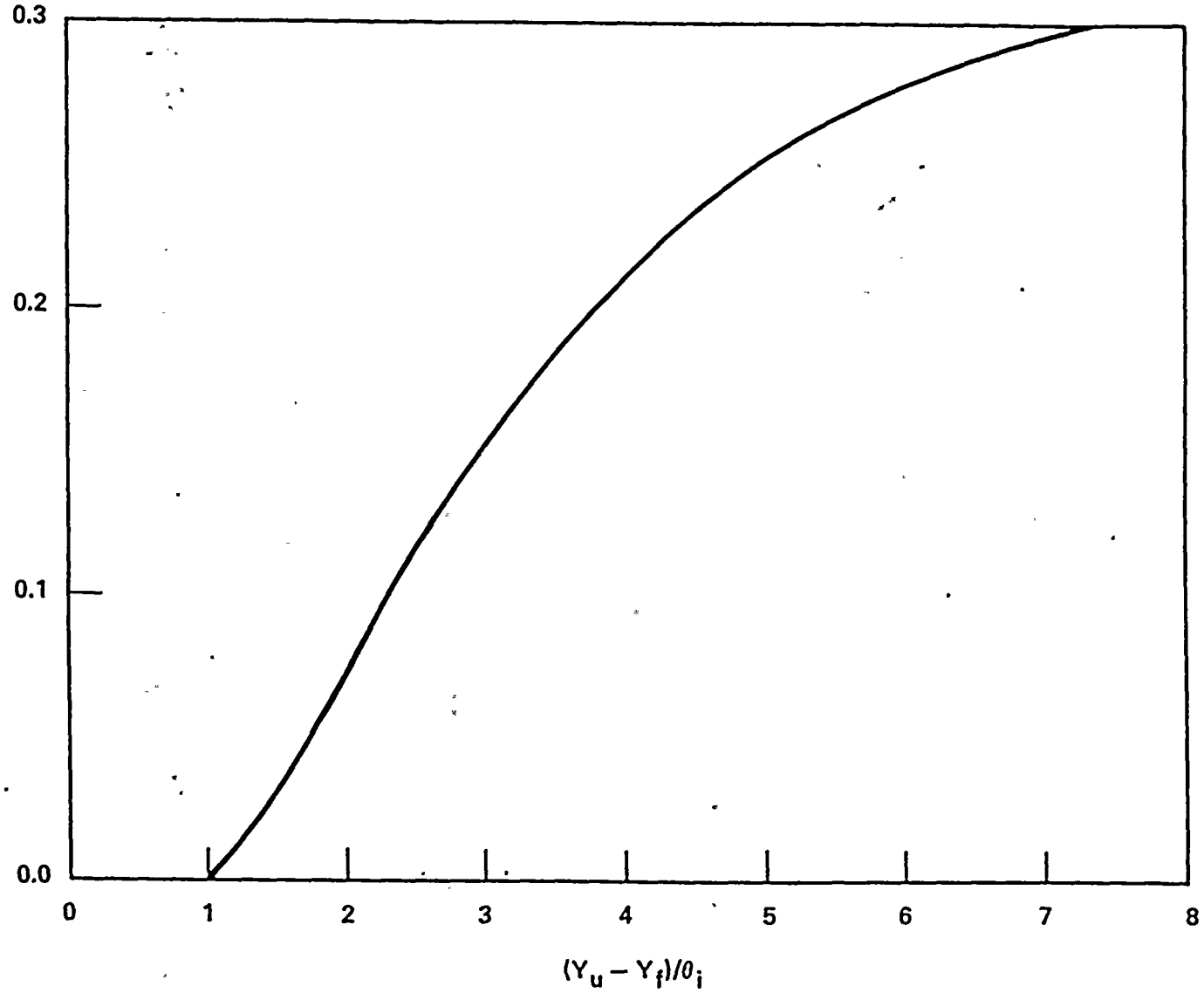

FIGURE 5.5 $(K)_{crit}\,\theta_i$ AT THE FLAMMABILITY LIMIT AS A FUNCTION OF $(Y_u - Y_f)/\theta_i$

flammability limit of hydrogen-air-steam mixtures[21]. The results indicated that most of the fog nozzles tested at 20°C only changed the limit from 4.03 volume percent to 4.76 percent, corresponding to fog concentration in the range of 0.028-0.085 volume percent, and average drop size ranging from 45-90 microns. For the 50°C case, the lower flammability limit increases to 7.2 percent, corresponding to 0.01-0.04 volume percent of fog and 20-50 micron average drop sizes. The results demonstrated that the fog inerting effect is more pronounced at small drop sizes.

Figures 5.6 through 5.8 show the comparison between the test data and the theoretical predictions. For this comparison, the present theory used the free stream temperature to calculate the thermodynamic properties used in Equation (5.5). This yielded somewhat higher fog concentrations than those calculated by use of the mean of the flame and free stream temperatures. In Figures 5.6 and 5.7, the data suggests a linear relationship between the volume concentration and volume mean drop size on the log-log plot. It also suggests that the minimum fog inerting concentration varies approximately with the square of the volume mean drop size. In this regard, the present theory is consistent with the data while the Berman et al. theory is not.

The present theory is in good agreement with the Factory Mutual data at 4.76 percent H_2; however, it overpredicts the minimum fog inerting concentration at 7.2 percent H_2. The cause of this discrepancy is still unknown. The discrepancy may be caused by the uncertainty of the data. The following discussion supports this claim. The fog droplets are very small and they vaporize very fast in a flame. Therefore, the fog droplets behave as steam except for their larger heat absorption capability. When the fog droplets vaporize, they absorb the heat of vaporization which is much larger than the steam sensible heat. Typically, the heat of vaporization of water is about 1000 Btu/lb and the average specific heat of steam in the temperature range of interest is about 0.48 Btu/lb. It is well known that a hydrogen flame cannot propagate in steam higher than about 64 percent in a steam-air mixture. At 7.9 H_2, the adiabatic flame temperature is about 1240°F and therefore

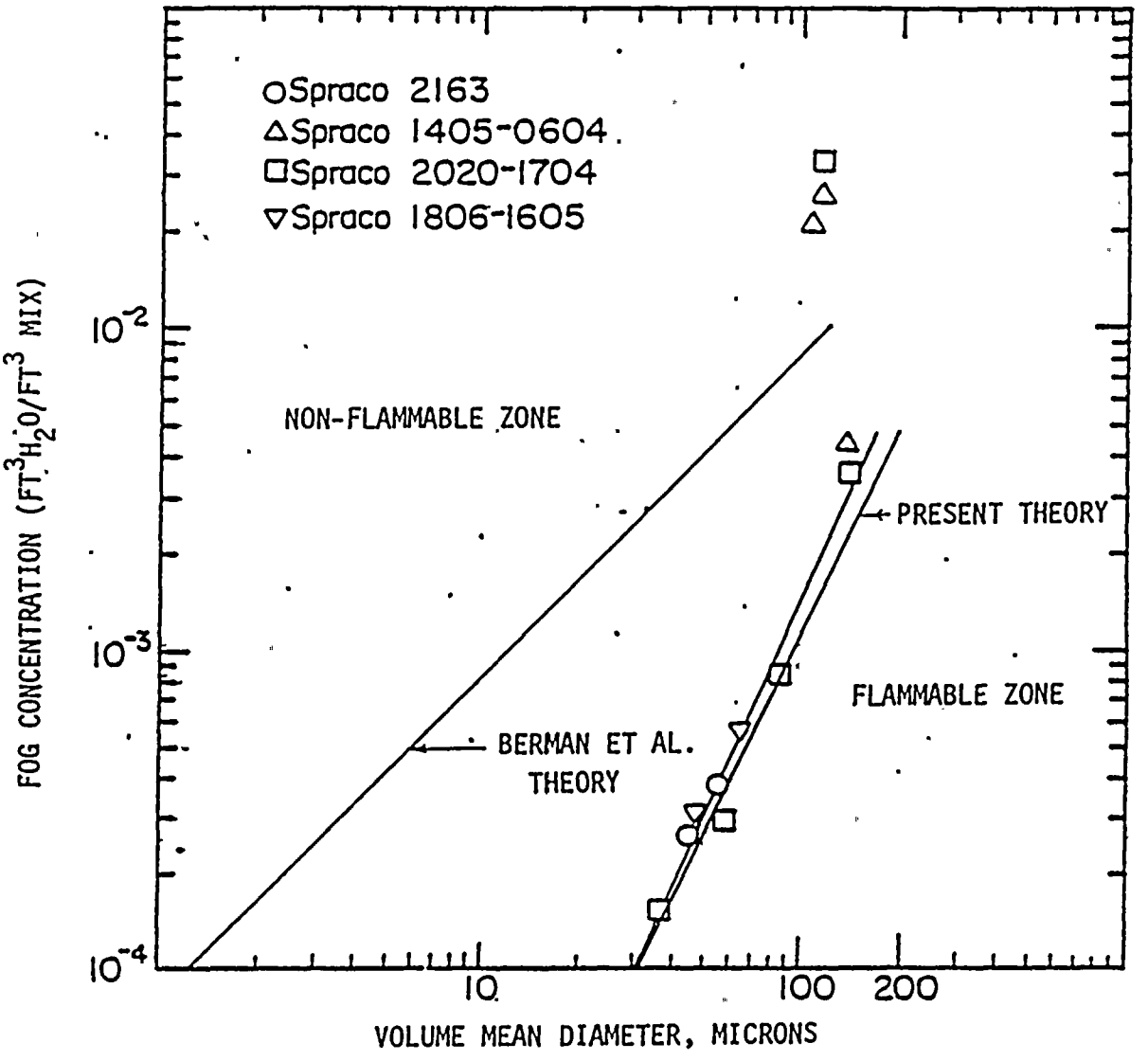

FIGURE 5.6 COMPARISON BETWEEN THEORIES AND FACTORY MUTUAL FOG INERTING EXPERIMENTS ON 4.76 PERCENT H_2

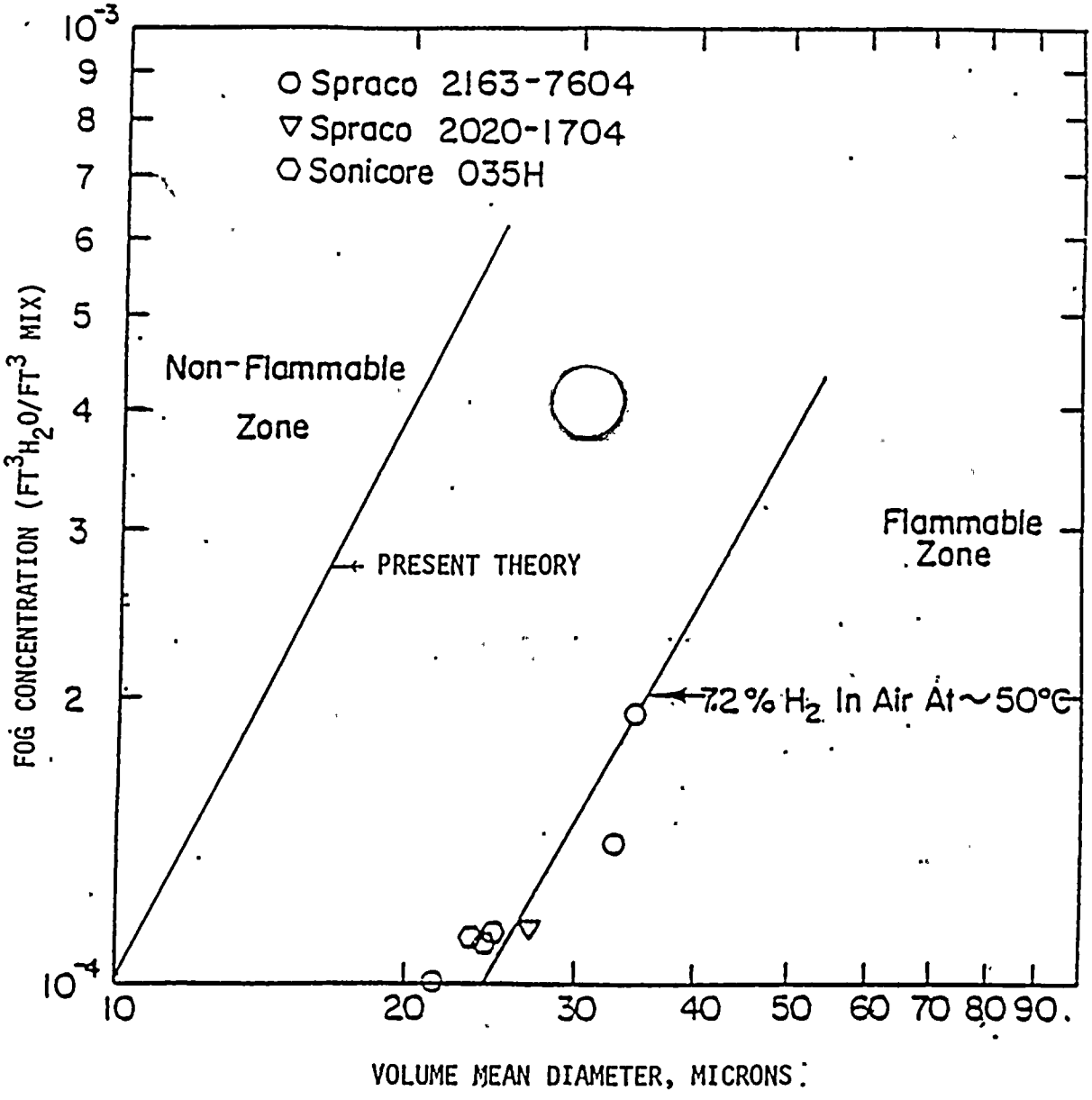

FIGURE 5.7 COMPARISON BETWEEN THE PRESENT THEORY AND FACTORY MUTUAL FOG INERTING EXPERIMENTS ON 7.2 PERCENT H_2

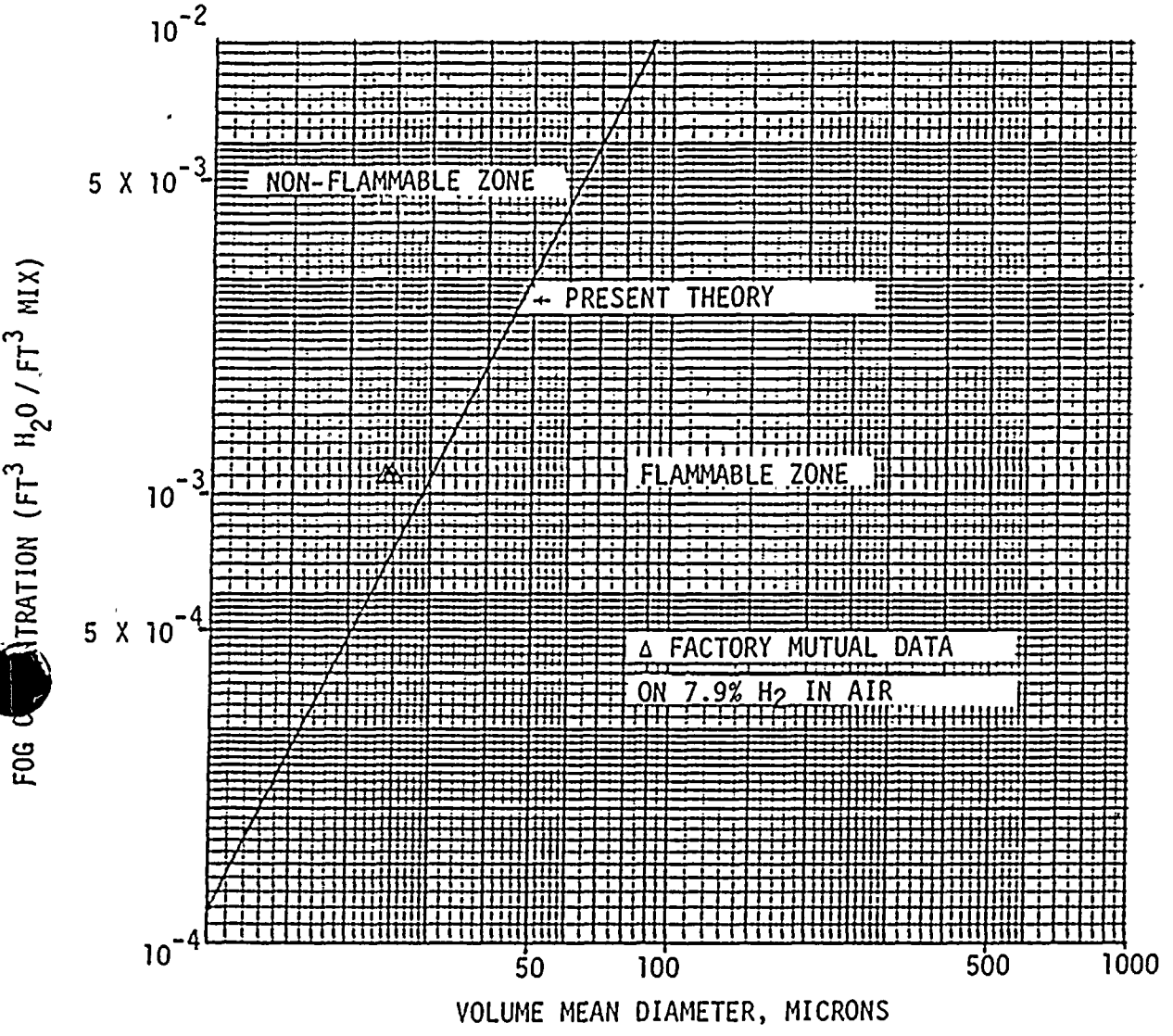

FIGURE 5.8 COMPARISON BETWEEN THE PRESENT THEORY AND FACTORY MUTUAL FOG INERTING EXPERIMENTS ON 7.9 PERCENT H_2

the increase of the steam sensible heat is about 540 Btu/lb. Consequently, for the same amount of fog droplets and steam, the fog droplets heat absorption capability is about 1.9 times higher. This means that the fog concentration which is equivalent to 22.1 percent steam in steam and air is capable of inerting 7.9 percent H_2. This fog inerting concentration was calculated to be 1.61×10^{-4}. To inert 7.2 percent H_2, a minimum fog concentration which corresponds to about 21.3 percent steam in steam and air is required. This gives a minimum fog inerting concentration of 1.56×10^{-4} for 7.2 percent H_2. These estimates show that the present predictions are reasonable and conservative. The present theory is conservative because it neglects convective and radiative heat transfer and thus underpredicts the heat loss. The estimates are consistent with Factory Mutual data on 7.9 percent H_2 but not on 7.2 percent H_2.

It should be noted that in the tests three fog concentration measuring techniques were used. These three techniques gave substantially different results. The discrepancy is at least one order of magnitude difference. The fog concentration data presented in Figures 5.6 through 5.8 were obtained from one of the techniques. In view of the uncertainty of the data, care must be exercised in using them for inerting analysis purposes. They should be used in conjunction with the present fog inerting criterion in the assessment of fog inerting potential in the ice condenser plants. Some uncertainty also exists in the present fog inerting theory. The uncertainty associated with the underprediction of the heat loss and temperature dependence of the thermophysical properties is estimated to be $\pm$63 percent.

It should also be pointed out that the Factory Mutual data and the present theory can only predict the minimum fog inerting concentration. To insure hydrogen burn in all directions in the ice condenser upper plenum, further work in this area may be required.

6.0 ASSESSMENT OF FOG INERTING PROBABILITY IN ICE CONDENSER CONTAINMENTS

As discussed in the previous sections, there exists several mechanisms of generating and removing fog droplets from the ice condenser containment. In addition, fog droplets are also transported from one subcompartment to another by entrainment in the gas stream. The fog entrainment rate is difficult to assess without knowing the velocity field and drop size distribution. For simplifying purposes, it is presently assumed that, the mass fraction of mist droplets in the intercompartmental and fan flows is the same as that within the subcompartment from which the flows are originated. This is a good assumption since the fog droplets are small. The amount of fog droplets in a subcompartment depends on all these mechanisms.

The total amount of fog droplets is important in determining the volume fraction of suspended condensate in a subcompartment. This volume fraction, in turn, is used in the fog inerting criteria to determine whether a particular hydrogen mixture composition formed in a subcompartment at any time is flammable or not. In other words, by knowing the hydrogen concentration and the mean fog drop size, we can determine whether the calculated volume fraction of fog droplets is high enough to prevent the mixture from combustion.

6.1 DETERMINATION OF VOLUME FRACTION OF MIST DROPLETS IN ICE CONDENSER CONTAINMENTS

Consider a subcompartment in the ice condenser comtainment as shown in Figure 6.1. There exist several mechanisms by which mist drops can be generated or removed. Fog droplets can be generated by homogeneous or heterogeneous nucleation in the thermal boundary layer and/or in the bulk stream and they can increase in size by condensation or decrease in size by vaporization. The rate of generation of mist droplets by condensation and their continued growth (or shrinkage due to vaporization) is represented by $\dot{m}_{cond}$. The other mechanism of generating mist droplets considered in this analysis is the primary coolant discharge from the break and the rate of generating fog droplets from this mechanism is

represented by $\dot{m}_{break}$. Two fog droplet removal mechanisms are considered in this analysis: one is gravitational settling and the other is removal by containment spray. The fog droplet removal rate by gravitational settling is represented by $\dot{m}_{set}$ and that by spray is represented by $\dot{m}_{sp}$. In addition to the generating and removal mechanisms discussed above, the mist droplet concentration in a subcompartment is also affected by the intercompartmental and fan flows. In the intercompartmental and fan flows, the mass fraction of fog droplets entrained is η and the gas mixture flow rate is $\dot{m}$. Therefore the rates of fog droplets mass into and out of a subcompartment are $\sum \eta_{in} \dot{m}_{in}$ and $\sum \eta_{out} \dot{m}_{out}$, respectively. It should be noted that $\sum \eta_{in} \dot{m}_{in}$ and $\sum \eta_{out} \dot{m}_{out}$ include the fog mass entrainment rates in all the intercompartmental and fan flows into and out of a subcompartment.

The mass conservation equation for the fog droplets in a subcompartment may be expressed as

$$\frac{dM_c}{dt} = \sum \eta_{in} \dot{m}_{in} - \sum \eta_{out} \dot{m}_{out} + \dot{m}_{break} + \dot{m}_{cond} - \dot{m}_{set} - \dot{m}_{sp} \quad (6.1)$$

where $\sum$ is a summation over all the flow paths. In Eq. (6.1), if m_{cond} is negative, then it becomes the rate of vaporization. Eq. (6.1) can be integrated to give the total mass of condensate at time t

$$M_c(t) = \int_0^t (\sum \eta_{in} \dot{m}_{in} - \sum \eta_{out} \dot{m}_{out} + \dot{m}_{break} + \dot{m}_{cond} - \dot{m}_{set} - \dot{m}_{sp})\, dt$$

$$\simeq \sum_i (\sum \eta_{in}^i \dot{m}_{in}^i - \sum \eta_{out}^i \dot{m}_{out}^i + \dot{m}_{break}^i + \dot{m}_{cond}^i - \dot{m}_{set}^i - \dot{m}_{sp}^i)\, \Delta t_i \quad (6.2)$$

The present analysis will employ the CLASIX calculations of containment transient during a small LOCA. In the CLASIX analysis, the entire ice condenser containment is usually divided into five or six subcompartments for analysis purposes. Temperatures, total pressure, steam partial pressures, and intercompartmental flow rates are calculated during transients. This information is used in Eq. (6.2) to determine fog droplet mass.

When applying Eq. (6.1) to each individual subcompartment, we have the following fog mass conservation equations in finite difference form:

Upper Compartment

$$M_{UC}(t+\Delta t) = M_{UC}(t) + \Big(\sum n_{in}\, \dot{m}_{in}(t) - \sum n_{out}\, \dot{m}_{out}(t) + \dot{m}_{UC,cond}(t) - \dot{m}_{UC,set}(t) - \dot{m}_{UC,sp}(t) \Big) \Delta t \qquad (6.3)$$

Lower Compartment

$$M_{LC}(t+\Delta t) = M_{LC}(t) + \Big(\sum n_{in}\, \dot{m}_{in} - \sum n_{out}\, \dot{m}_{out} + \dot{m}_{LC,break}(t) - \dot{m}_{LC,cond}(t) - \dot{m}_{LC,set}(t) - \dot{m}_{LC,sp}(t) \Big) \Delta t \qquad (6.4)$$

Ice Condenser Upper Plenum

$$M_{UP}(t + \Delta t) = M_{UP}(t) + (\sum n_{in}\, \dot{m}_{in}(t) - \sum n_{out}\, m_{out}(t) + \dot{m}_{UP,cond}(t) - \dot{m}_{UP,set}(t)) \quad \Delta t$$

Ice Condenser Lower Plenum

$$M_{LP}(t + \Delta t) = M_{LP}(t) + \left(\sum n_{in}\, \dot{m}_{in}(t) - \sum n_{out}\, \dot{m}_{out}(t) + \dot{m}_{LP,cond}(t) - \dot{m}_{LP,set}(t) \right) \Delta t \qquad (6.5)$$

Dead Ended Region

$$M_{DE}(t + \Delta t) = M_{DE}(t) + \left(\sum n_{in}\, \dot{m}_{in}(t) - \sum n_{out}\, \dot{m}_{out}(t) + \dot{m}_{DE,cond}(t) - \dot{m}_{DE,set}(t) \right) \Delta t \qquad (6.6)$$

Fan/Accumulator Rooms*

$$M_{FA}(t + \Delta t) = M_{FA}(t) + \left(\sum n_{in}\, \dot{m}_{in}(t) - \sum n_{out}\, \dot{m}_{out}(t) + \dot{m}_{FA,cond}(t) - \dot{m}_{FA,set}(t) - \dot{m}_{FA,sp}(t) \right) \Delta t \qquad (6.7)$$

In the present analysis, the fog concentrations in the intercompartmental and fan flows are assumed to be the same as those in the compartment from which the flows are orginated.

---

* These rooms were analyzed only for the D. C. Cook plant (See Figure 6.9).

In the equations given above, the intercompartmental and fan flow rates $\dot{m}_{in}$ and $\dot{m}_{out}$ are provided by CLASIX calculational results. The procedures of calculating fog droplets generating and removal rates are based on the discussions in the previous sections and the details are given in the following sections.

6.1.1 CALCULATION OF $\dot{M}_{BREAK}$

To date little experimental data is available to estimate the amount of fog droplets generated by the break flow. For a large LOCA, Almenas and Marchello[3] estimated that 13 percent of the total blowdown drop population (by weight) has drop radius range from 1 μ to 20 μ and only 1 percent less than 1 μ. This estimate is somewhat larger than the 4 μ mean drop size sited in Section 3.1.2, which is believed to be conservative.

Since we are only interested in fog drops smaller than 20 μ, and only these drops can remain suspended in air until the time when the hydrogen is released, we assume that the estimate of Almenas and Marchello is applicable in small LOCAs and 14 percent of the suspended liquid are fog droplets which have a potential inerting effect.

The fraction of reactor coolant discharged from the break remains as suspended liquid has been determined in Section 3. Knowing the break flow rates from a computer code such as MARCH, we can calculate the amount of liquid suspended in the atmosphere. Then from the drop size distribution we can calculate the amount of fog droplets suspended in the atmosphere.

Defining the blowdown rate as $\dot{m}_b$, the liquid fraction of the break flow as ξ_b, the fraction of fog droplets smaller than 20 μ as f_b, we have

$$\dot{m}_{break} = f_b \dot{m}_b \xi_b \tag{6.8}$$

In the present analysis $f_b = 0.14$ is used. f_b becomes zero when the water level in the reactor vessel falls below the break elevation.

6.1.2 CALCULATION OF $\dot{M}_{COND}$

As discussed previously, $\dot{m}_{cond}$ is the rate of formation of mist droplets by nucleation, condensation, or vaporization. Nucleation of fog droplets can take place in the thermal boundary layer and in the bulk fluid. We conservatively assume that little supersaturation is needed for nucleation in the bulk stream and fog will form when the bulk stream steam partial pressure reaches the saturation steam pressure corresponding to the gas stream temperature. Therefore, the bulk stream fog formation rates can be determined from the equilibrium thermodynamic states of the gas mixture.

The boundary layer fog formation rate can be determined using the Hijikata-Mori theory[17] of fog formation in the thermal boundary layer as discussed in Section 3.2.4. The fog formation rate in the thermal boundary layer and the bulk stream is given by Eq. (3.12). Boundary layer and bulk stream fog formation rates will be calculated for the ice condenser and lower compartment.

A computer program called FOG has been developed to calculate $\dot{m}_{cond}$. This computer program requires input of the volumetric gas flow rate, gas and wall temperatures, total pressure, and steam partial pressure. This information can be obtained from the CLASIX output.

6.1.3 CALCULATION OF $\dot{M}_{SET}$

The rate of settling of the fog droplets depends on their terminal velocity, concentration and compartment cross sectional area. The droplet terminal velocity is a function of drop size. In the present study, Equation (4.1) will be used to calculate the fog gravitational settling rate.

6.1.4 CALCULATION OF $\dot{M}_{SP}$

The mass of a fog droplet is much smaller than that of a spray droplet. Therefore, when a spray droplet collides with a fog droplet, the fog droplet will coalesce with the spray drop and fall to the sump. In the present study, the fog removal rate by sprays is given by Equation (4.2).

It is expected that the spray drop collection efficiency is very high, and therefore a 100 percent drop collection efficiency is assumed in the analysis. A sensitivity study is needed to be carried out to study the effect of E on the volume fraction of fog droplets.

A computer program called FOGMASS has been developed to solve Eqs. (6.3) through (6.7). This program uses a finite difference numerical scheme to carry out integration. This program takes input from FOG and CLASIX output data. Specific output data from CLASIX are time histories of gas temperature, wall temperature, total pressure, steam partial pressure, and intercompartmental and fan flow rates.

6.2 FOG INERTING PROBABILITY IN THE SEQUOYAH PLANT

The computer codes, FOG and FOGMASS, were used to perform fog inerting analysis for the Sequoyah plant. FOG was used to calculate the rates of fog formation due to boundary layer and bulk stream condensation in the Sequoyah ice condenser and lower plenum. Then these fog formation rates were used in FOGMASS to compute the fog concentrations in each of the Sequoyah containment subcompartments.

To compute the fog formation rates in the ice condenser upper plenum and lower compartment, some output data from the Sequoyah CLASIX analysis[27] are needed. These data include time histories of gas temperature, wall temperature, total pressure, and steam partial pressure in each containment subcompartment, as well as the intercompartmental and fan flow rates. In order to utilize the CLASIX output data, the ice condenser containment is subcompartmentalized in the FOGMASS program in exactly the same manner as in Reference 27. The subcompartmentalization model used in the Sequoyah CLASIX analysis is shown in Figure 6.1. In this study only the S_2D accident scenario has been analyzed.

FIGURE 6.1 SEQUOYAH CLASIX CONTAINMENT MODEL

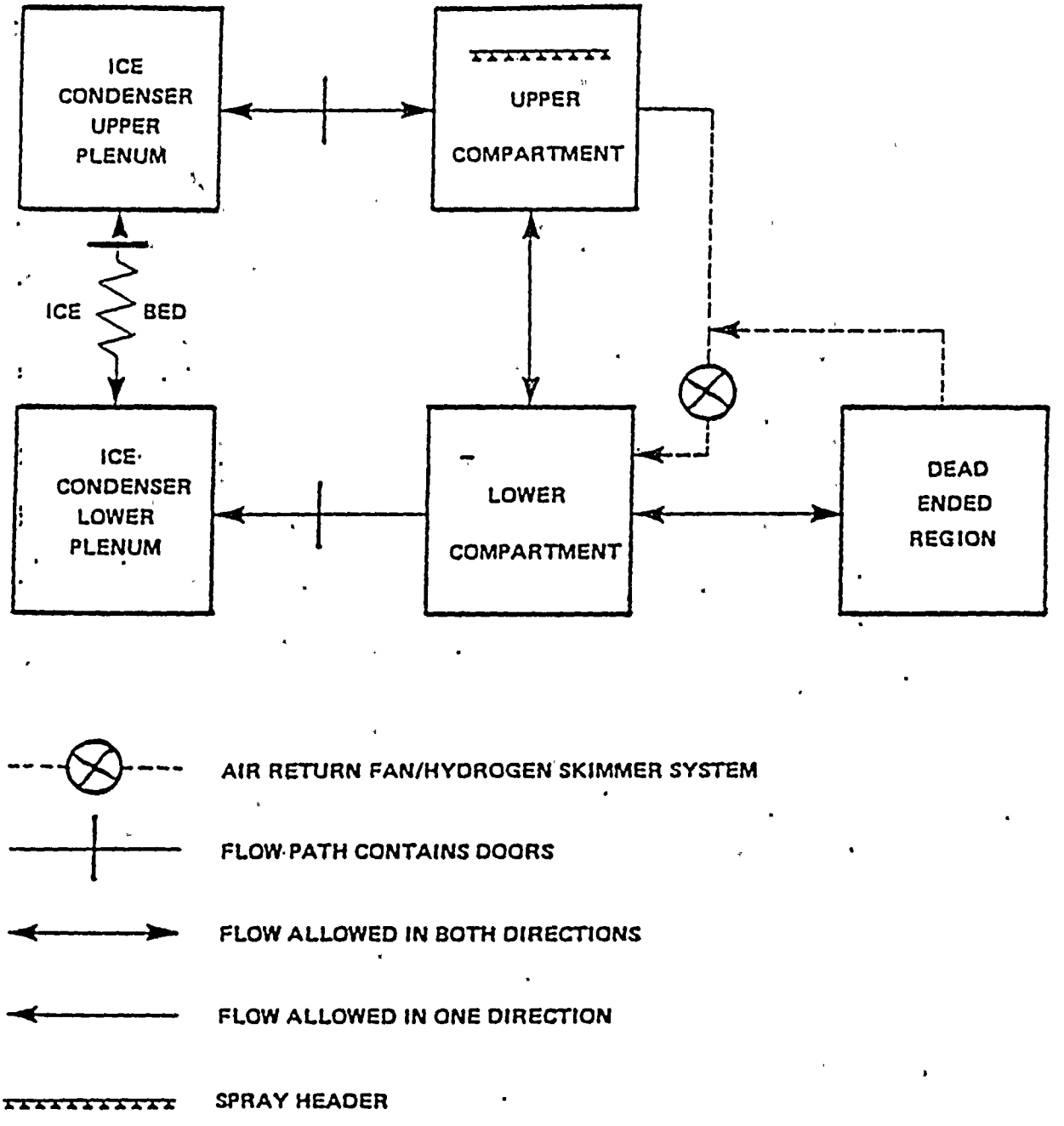

The FOG input data for Sequoyah S_2D Case 1 are given in Tables 6.1 and 6.2, and the calculational results are shown in Figures 6.2 and 6.3. In Figure 6.2, the fog formation rate in the lower compartment is shown. For the first few hundred seconds the wall temperature is lower than the dew point corresponding to the steam partial pressure and therefore fog starts to form. After about 600 seconds, the fog formation rate becomes negligibly small since the wall temperature is only a few degrees below the dew point. There is no fog formation in the lower compartment after about 1800 seconds. The fog formation rate in the ice condenser is shown in Figure 6.3. It is seen that the fog formation rate in the ice condenser is much larger than that in the lower compartment. It increases with the ice condenser steam flow rate and reaches a peak of 14 lb/sec at about 1800 seconds. The fog formation rate in the ice condenser then begins to decrease and is low at the time of significant hydrogen release.

The nine fog formation rates in the lower compartment and in the ice condenser are input to FOGMASS in a tabular form and there is a built-in interpolation scheme in FOGMASS to obtain values for the intermediate time steps.

FOGMASS computes the rate of fog generation by the break flow, the fog settling rate due to gravity, and the fog removal rate due to sprays, as well as the rates of fog entrainment by intercompartmental and fan flows. The input data needed to calculate each of these rates are discussed as follows.

The rate of reactor coolant release to the containment and the coolant enthalpy were obtained from the MARCH output[7] for a small LOCA. The quality of the break flow was calculated using the enthalpy and the lower compartment gas temperature. According to the MARCH prediction[7] the discharge of liquid by the break flow into the lower compartment lasts for only 2172 seconds. Afterward, the water level in the reactor vessel drops below the break elevation and the fluid discharged

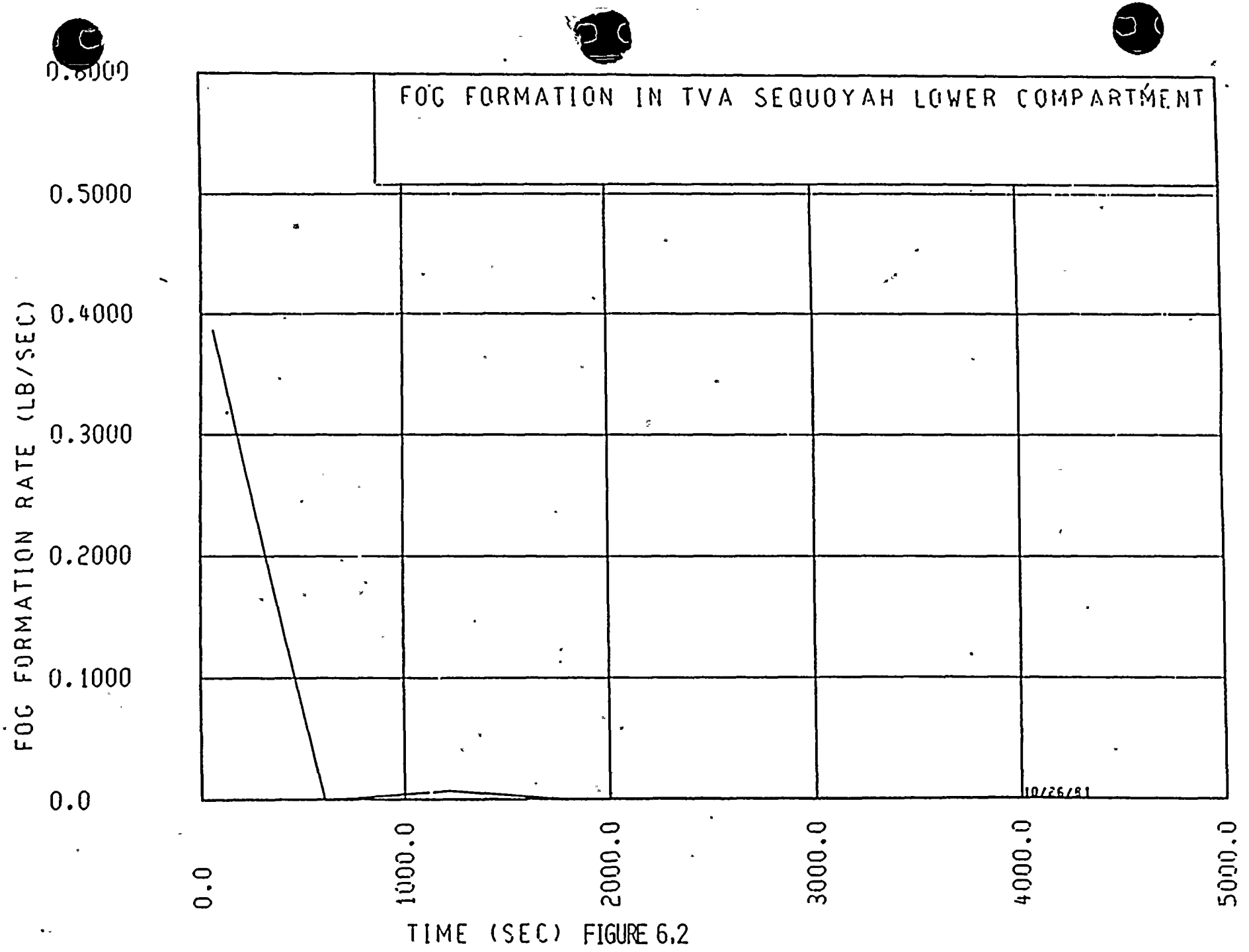
FOG FORMATION IN TVA SEQUOYAH LOWER COMPARTMENT
FOG FORMATION RATE (LB/SEC)
0.6000
0.5000
0.4000
0.3000
0.2000
0.1000
0.0
0.0
1000.0
2000.0
3000.0
4000.0
5000.0
TIME (SEC)
10/26/81

FIGURE 6.2

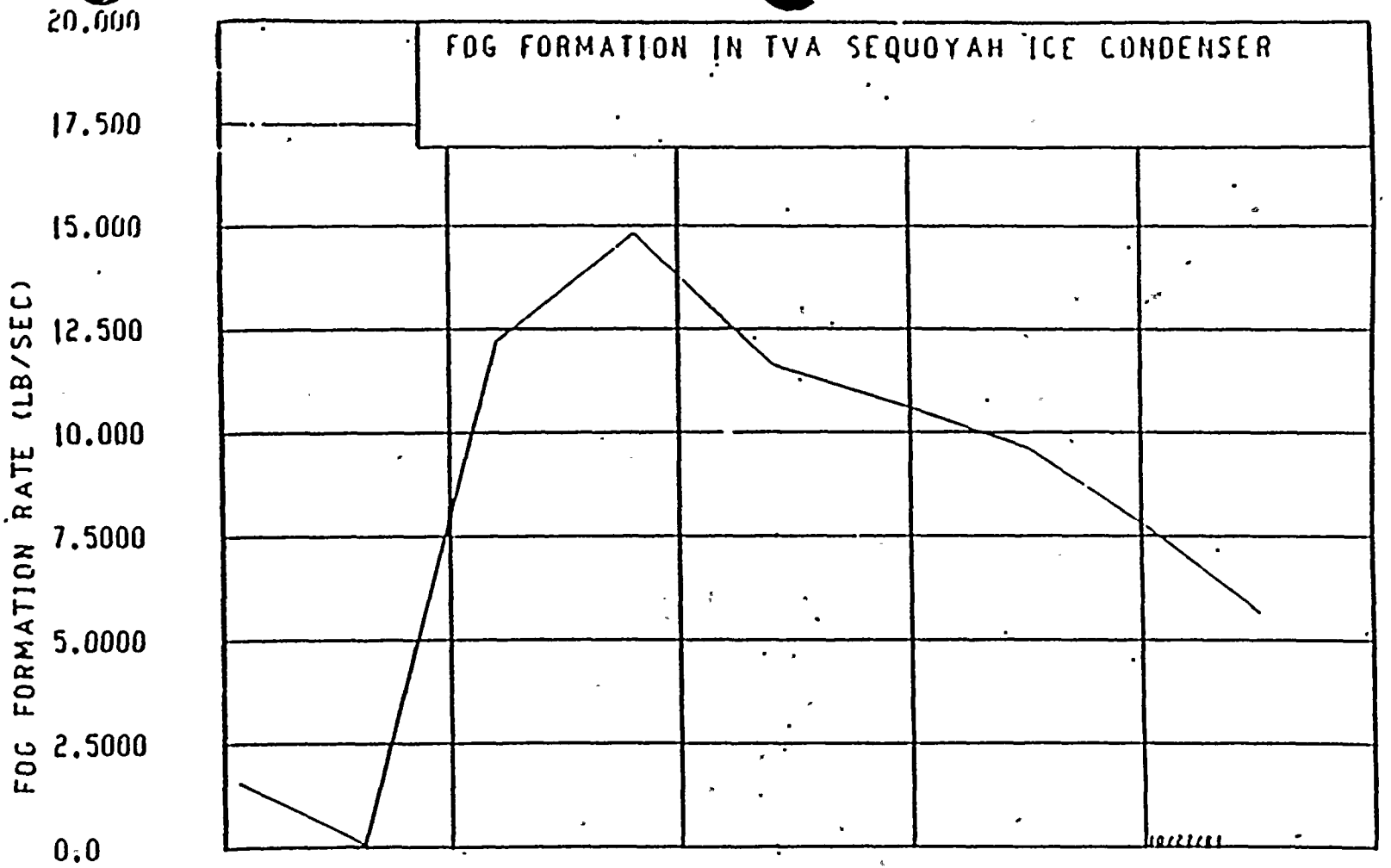

FIGURE 6.3 FOG FORMATION IN TVA SEQUOYAH ICE CONDENSER

from the break is essentially steam. Therefore, in the present study, it is assumed that no fog is generated by the break flow after 2172 seconds.

For fog removal by gravitational settling, a volume mean drop size of 10 μ was assumed. The terminal velocity of a 10 μ drop is about 1 cm/sec. Because of this low terminal velocity, gravitational settling is not an effective fog removal mechanism. The assumption of 10 μ volume mean drop size is therefore conservative, considering the fact that for a few thousand seconds the drop agglomeration mechanism would be able to increase volume mean drop size substantially. It should also be noted that a smaller volume mean drop size means that the minimum fog inerting concentration would be reduced and thus makes the present analysis conservative. Furthermore, no consideration was given to the deposition of fog on the walls and vertical surfaces of the structure, or for fog removal in the fan flows when it passes through ducts and fans. All the assumptions mentioned above make the present analysis very conservative. The containment geometric data needed in computing the settling rate are given in Table 6.3.

For fog removal by sprays, a spray flow rate of 9500 gpm was used for Sequoyah. According to the Sequoyah CLASIX analysis[27], the sprays are initiated at 142 seconds. A volume fraction of sprays (volume of sprays divided by volume of the spray zone) of 3.3×10^{-4} was used, which was obtained using a spray drop fall height of 107 ft, a spray zone volume of 485,500 ft^3, and a volume mean drop size of 700 μ. As previously discussed a spray removal of a 100 percent was used.

In Figure 6.1, the directions of the intercompartmental flows are shown. The intercompartmental flow rates for the six flow paths and nine time steps were obtained from the OPS CLASIX analysis and are given in Table 6.5. The present analysis considers the intercompartmental flows as the mechanisms of transporting fog from one compartment to another. It was assumed in the present analysis that the fog concentrations in the intercompartment flows are the same as those in the compartments from which the flows are originated.

It is seen in Figure 6.1 that two trains of the air return fan and hydrogen skimmer system take suction from the dead ended region and from the upper compartment and discharge into the lower compartment. The fans are initiated at 712 seconds. The fan head-flow curve reported in Reference 27 was used to compute the fan flow rates. Fan flow rates of 1645 ft^3/sec and 10 ft^3/sec were used for the air return fan and the hydrogen skimmer system, respectively. These flow rates were calculated using average Δp's between the upper compartment and the lower compartment, and between the dead ended region and the lower compartment. It was also assumed that the fog concentrations in the fan flows are the same as those in the compartments from which the flows are originated.

The results of the FOGMASS calculation are shown in Figure 6.4. It is seen that for the first few hundred seconds the fog concentrations in the lower compartment, ice condenser lower and upper plenums are about the same and increasing. At about 700 seconds, the lower compartment fog concentration reaches its peak of 2.2×10^{-4}. Afterward, the intercompartmental flows transport more fog droplets out of the lower compartment than are generated by the break flow and condensation and, therefore, the lower compartment fog concentration decreases. However, the upper plenum fog concentration keeps rising until about 900 seconds, due to an increasing fog formation in the ice condenser and more fog entrained in the intercompartmental flow into the upper plenum. The upper plenum fog concentration reaches its peak of 5.4×10^{-4} at about 900 seconds. The lower plenum fog concentration is almost the same as the lower compartment fog concentration because of little difference in the intercompartmental flow rates into and out of the ice condenser lower plenum. Therefore, these two volumes behave as a single volume in terms of fog concentration.

At 2172 seconds, the break flow in the lower compartment stops generating fog and, therefore, the fog concentrations drop sharply thereafter. The effect is more pronounced for the lower compartment and lower plenum fog concentrations. The highest fog concentration exists in the ice condenser upper plenum while the lowest exists in the upper compartment. The effect of sprays on the upper compartment fog concentration is clearly seen in Figure 6.4. At 142 seconds, the sprays are

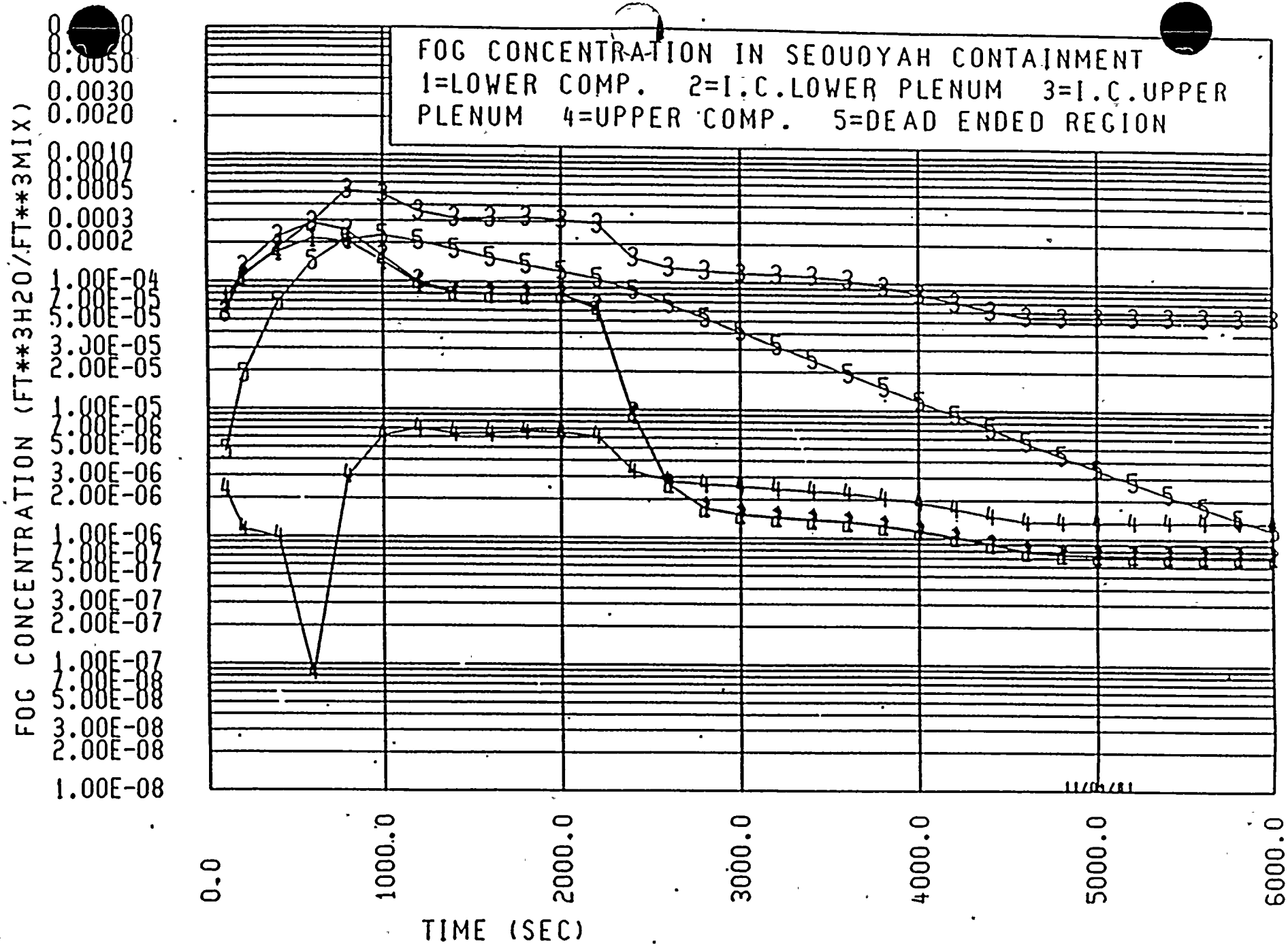
FOG CONCENTRATION IN SEQUOYAH CONTAINMENT
1=LOWER COMP. 2=I.C.LOWER PLENUM 3=I.C.UPPER PLENUM 4=UPPER COMP. 5=DEAD ENDED REGION
FOG CONCENTRATION (FT**3H2O/FT**3MIX)
0.0050
0.0030
0.0020
0.0010
0.0007
0.0005
0.0003
0.0002
1.00E-04
2.00E-05
5.00E-05
3.00E-05
2.00E-05
1.00E-05
2.00E-06
5.00E-06
3.00E-06
2.00E-06
1.00E-06
2.00E-07
5.00E-07
3.00E-07
2.00E-07
1.00E-07
2.00E-08
5.00E-08
3.00E-08
2.00E-08
1.00E-08
0.0
1000.0
2000.0
3000.0
4000.0
5000.0
6000.0
TIME (SEC)

FIGURE 6.4

turned on and the upper compartment fog concentration drops sharply until about 600 seconds. At about 600 seconds, the upper compartment fog concentration starts to increase again because the intercompartmental flow into the compartment increases sharply at that time. A peak concentration of 7×10^{-6} in the upper compartment is reached at about 1200 seconds.

Hydrogen starts to release into the containment at about 3804 seconds, according to the MARCH calculation[27]. It reaches 4 volume percent at about 4300, 4400, and 4670 seconds in the lower compartment, upper plenum, and upper compartment, respectively.

At 4300 seconds, the calculated lower compartment fog concentration is 9.7×10^{-7}, which is about an order of magnitude smaller than the minimum fog concentrations required for inerting 4 percent H_2. At 4670 seconds, the upper compartment fog concentration is 1.35×10^{-6}, which is about a factor of five smaller than the minimum fog concentration required for inerting 4 percent H_2*. At the times of reaching 8.5 percent H_2, the fog concentrations in the lower and upper compartments are even lower than the figures given above. Therefore, it is concluded that the fog concentrations in the lower and upper compartments are too low to have any inerting effect. The use of the present theory on fog inerting also leads to the same conclusion.

However, at 4400 seconds, the calculated fog concentration in the upper plenum is 6.1×10^{-5} which is higher than the Factory Mutual fog inerting data extrapolated to 10 μ drops and the present theoretical prediction. The data shows that in order to inert 4.76 percent H_2 the fog concentration must be 8.4×10^{-6} or higher for 10 μ volume mean drop size. At 4600 seconds, the upper plenum hydrogen concentration reaches about 7 percent and the fog concentration is 5.5×10^{-5}. Again, an extrapolation of the Factory Mutual data to 10 μ shows that fog concentration of 2.1×10^{-5} or higher is required to inert 7.2 percent H_2. In comparison, the present theory on fog inerting predicts 1.02×10^{-4} for 7.2 percent H_2.

---

* The fog inerting criterion used is described in Section 5.2.

Therefore, it appears that it is possible to inert 7 percent H_2 but unlikely. However, at 8 percent H_2 in the upper plenum, which occurs at about 4650 seconds, the fog concentration is 5.5×10^{-5}, which is too low to inert 8 percent H_2. An extrapolation of the Factory Mutual 8 percent H_2 data to 10 μ volume mean drop size and the present prediction give 1.9×10^{-4} and 1.2×10^{-4} for the minimum required fog inerting concentration, respectively. Therefore both the theory and the extrapolation of test data show that fog inerting will not occur in the upper plenum.

The glow plug igniters which have been installed in the Sequoyah containment were designed to burn hydrogen lower than 8.0 percent. As discussed previously, no fog inerting effects will be expected in the Sequoyah lower and upper compartments. Therefore, the glow plug igniters are expected to function as designed in these two compartments. It may be possible that fog present in the ice condenser upper plenum may prevent the glow plug igniters from igniting hydrogen below 7 percent. However, it seems very unlikely that the same igniters would fail to ignite 8.0 percent H_2 as designed, considering the fact that considerable conservatism has been exercised in the present analysis.

Sensitivity studies of the spray removal efficiency and the fraction of blowdown droplets smaller than 20 μ for the Sequoyah plant have been performed. A case of 10 percent spray removal efficiency was run using FOGMASS. The calculational results showed that the fog concentrations in the lower compartment, lower plenum, and upper compartment at 4600 seconds were increased approximately by a factor of 10. However, these concentrations are still too low to inert 8 percent hydrogen. In comparison, the fog concentration in the upper plenum is increased by only 20 percent because the concentration at this time is primarily determined by the fog formation rate in the ice condenser. This increase is too small to change the conclusion given previously on the inerting probability in the upper plenum. Another case in which all the blowdown droplets were assumed to be smaller than 20 μ was run using FOGMASS. The calculational results showed that at 4600 seconds the fog concentrations in the lower compartment and lower plenum were increased by 15

percent while the increases in the upper plenum and upper compartment were negligibly small. The insensitivity of the fog concentrations to the parameter of the fraction of blowdown droplets smaller than 20 μ is due to the effectiveness of the spray removal. At 4600 seconds, almost all the blowdown droplets are removed by the sprays. The sensitivity studies showed that the fog concentration in the upper plenum at the time of significant hydrogen release is not sensitive to the spray removal efficiency and the fraction of blowdown droplets smaller than 20 μ.

TABLE 6.1 FOG INPUT DATA FOR SEQUOYAH LOWER COMPARTMENT

Time (sec)	Lower Compartment Gas Flow Rate (ft^3/sec)	Gas Temp. (°F)	Wall Temp. (°F)	Total Pressure (psia)	Steam Partial Pressure (psia)
60	1404.5	150	118	16.7	5
610	646.7	215	202	21.6	15.3
1210	3157.2	188	176	20.4	8.9
1810	3115.5	188	176	20.5	8.8
2410	2913.7	180	173	20.1	7.5
3010	2871.7	179	169	19.9	7.2
3510	2739.3	178	169	19.9	6.9
4010	2755.9	175	164	19.4	5.5
4510	2848.8	197	173	19.8	4.8

TABLE 6.2 FOG INPUT DATA FOR SEQUOYAH ICE CONDENSER

Time (sec)	Ice Condenser Gas Flow Rate (ft^3/sec)	Gas Temp. (°F)	Ice Temp. (°F)	Total Pressure (psia)	Steam Partial Pressure (psia)
60	1082	120	32	16.6	2.5
610	96.4	132	32	21.8	2.3
1210	2654	186	32	20.4	8.1
1810	2799	188	32	20.5	8.8
2410	2679	182	32	20.0	7.6
3010	2629	179	32	19.9	7.2
3510	2502	178	32	19.9	7.0
4010	2594	171	32	19.4	5.7
4510	2628	187	32	19.8	4.7

TABLE 6.3 GEOMETRIC DATA FOR SEQUOYAH CONTAINMENT

	Volume (ft^3)	Floor Area (ft^2)
Lower Compartment	289,000	5,410
Ice Condenser Lower Plenum	24,200	3,100
Ice Condenser Upper Plenum	47,000	3,200
Upper Compartment	651,000	10,390
Dead Ended Region	94,000	3,350

TABLE 6.4 MARCH PREDICTION OF REACTOR COOLANT MASS AND ENERGY RELEASE RATE FOR THE S_2D SEQUENCE

Time (seconds)	H_2O Mass Release Rate (lbm/sec)	H_2O Energy Release Rate (Btu/sec)
0.0	197.2	1.167×10^5
2172	190.5	1.097×10^5
2478	44.85	5.230×10^4
3180	53.53	6.547×10^4
3804	34.82	4.262×10^4
4428	21.40	2.842×10^4
4752	48.42	5.558×10^4
5700	19.42	2.182×10^4
6012	14.07	1.583×10^4
6960	5.253	5.989×10^3
7062	4.718	5.388×10^3
7206	4.060	4.693×10^3

TABLE 6.5 INTERCOMPARTMENTAL FLOW RATES (ft^3/sec) PREDICTED BY CLASIX FOR SEQUOYAH

Time (sec)	Flow From LC to LP	Flow From LP to UP	Flow From UP to UC	Flow From UC to LC	Flow From DE to LC
6.001E1	1.175E3	1.082E3	7.029E2	-9.905E1	-1.304E2
6.100E2	3.580E2	9.641E1	-3.931E1	-2.113E1	-2.676E2
1.210E3	2.864E3	2.654E3	1.272E3	-1.838E2	-1.094E2
1.810E3	2.828E3	2.799E3	1.323E3	-1.793E2	-1.088E2
2.410E3	2.695E3	2.679E3	1.375E3	-1.502E2	-6.855E1
3.010E3	2.654E3	2.629E3	1.407E3	-1.634E2	-6.326E1
3.510E3	2.528E3	2.502E3	1.352E3	-1.643E2	-4.699E1
4.010E3	2.613E3	2.594E3	1.537E3	-1.095E2	-3.348E1
4.510E3	2.694E3	2.628E3	1.627E3	-1.106E2	-4.426E1

6.3 FOG INERTING PROBABILITY IN THE McGUIRE PLANT

The computer codes, FOG and FOGMASS, were used to perform fog inerting analysis for the McGuire plant. FOG was used to calculate the rates of fog formation due to boundary layer and bulk stream condensation in the McGuire ice condenser and lower plenum. Then these fog formation rates were used in FOGMASS to compute the fog concentrations in each of the McGuire containment subcompartments.

To compute the fog formation rates in the ice condenser upper plenum and lower compartment, some output data from the McGuire CLASIX analysis[28] are needed. These data include time histories of gas temperature, wall temperature, total pressure, and steam partial pressure in each containment subcompartment, as well as the intercompartmental and fan flow rates. In order to utilize the CLASIX output data, the ice condenser containment is subcompartmentalized in the FOGMASS program in exactly the same manner as in Reference 28. The subcompartmentalization model used in the McGuire CLASIX analysis is shown in Figure 6.5. In this study only the S_2D accident scenario has been analyzed by CLASIX for McGuire.

The FOG input data for McGuire S_2D Case 1 are given in Tables 6.6 and 6.7, and the calculational results are shown in Figures 6.6 and 6.7. In Figure 6.6, the fog formation rate in the lower compartment is shown. For the first few hundred seconds the wall temperature is lower than the dew point corresponding to the steam partial pressure and therefore fog starts to form. The fog formation rate is low because the wall temperature is only a few degrees below the dew point. Fog formation in the lower compartment becomes zero after about 600 seconds. The fog formation rate in the ice condenser is shown in Figure 6.7. It is seen that the fog formation rate in the ice condenser is much larger than that in the lower compartment. The fog formation rate increases with the ice condenser steam flow rate and reaches the first peak at about 1510 seconds. Then the rate decreases because of the decrease in the steam flow rate. The fog formation and the steam flow rates start to increase again at about 2510 seconds. The fog formation rate reaches the second

FIGURE 6.5 MCGUIRE CLASIX CONTAINMENT MODEL

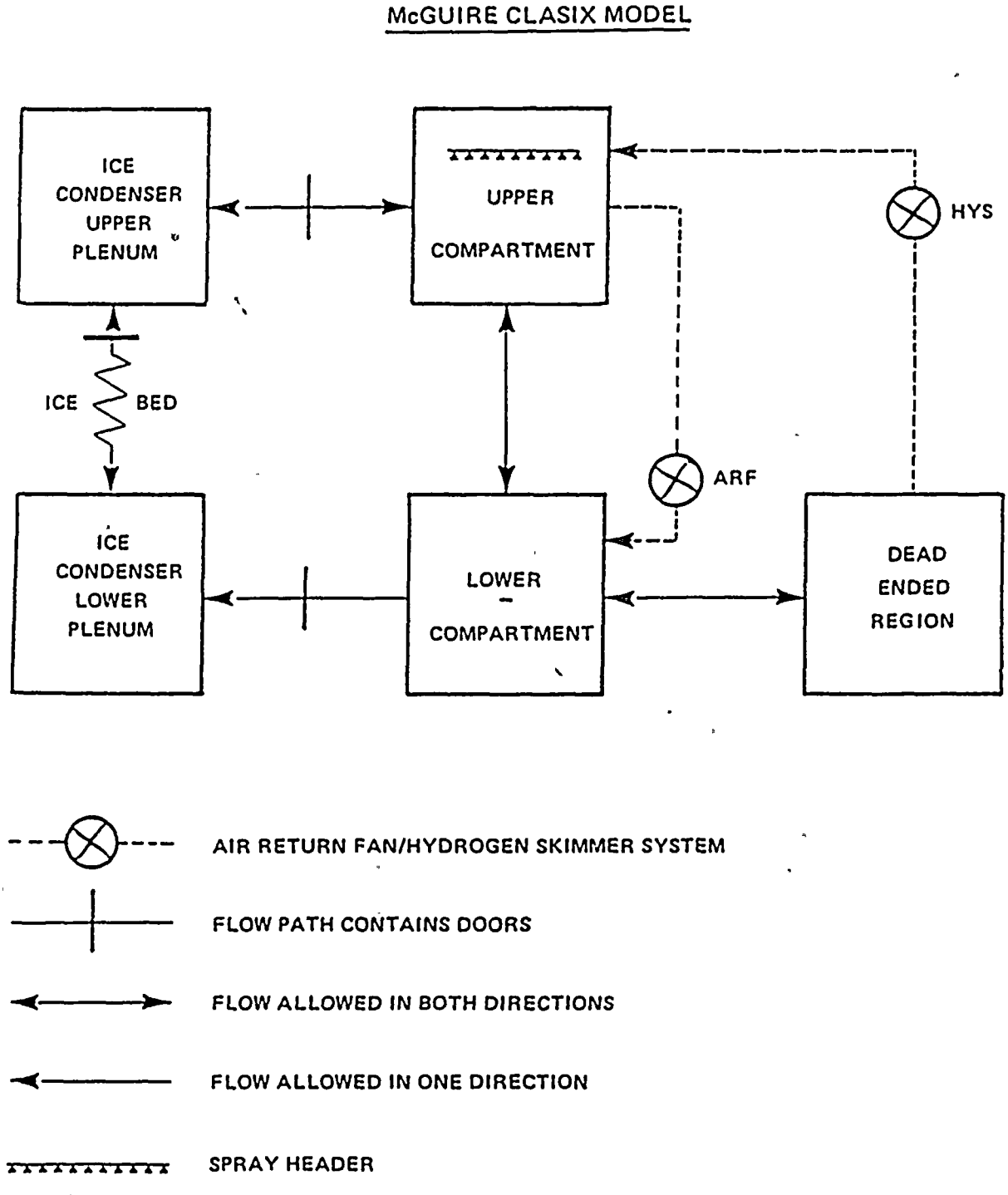

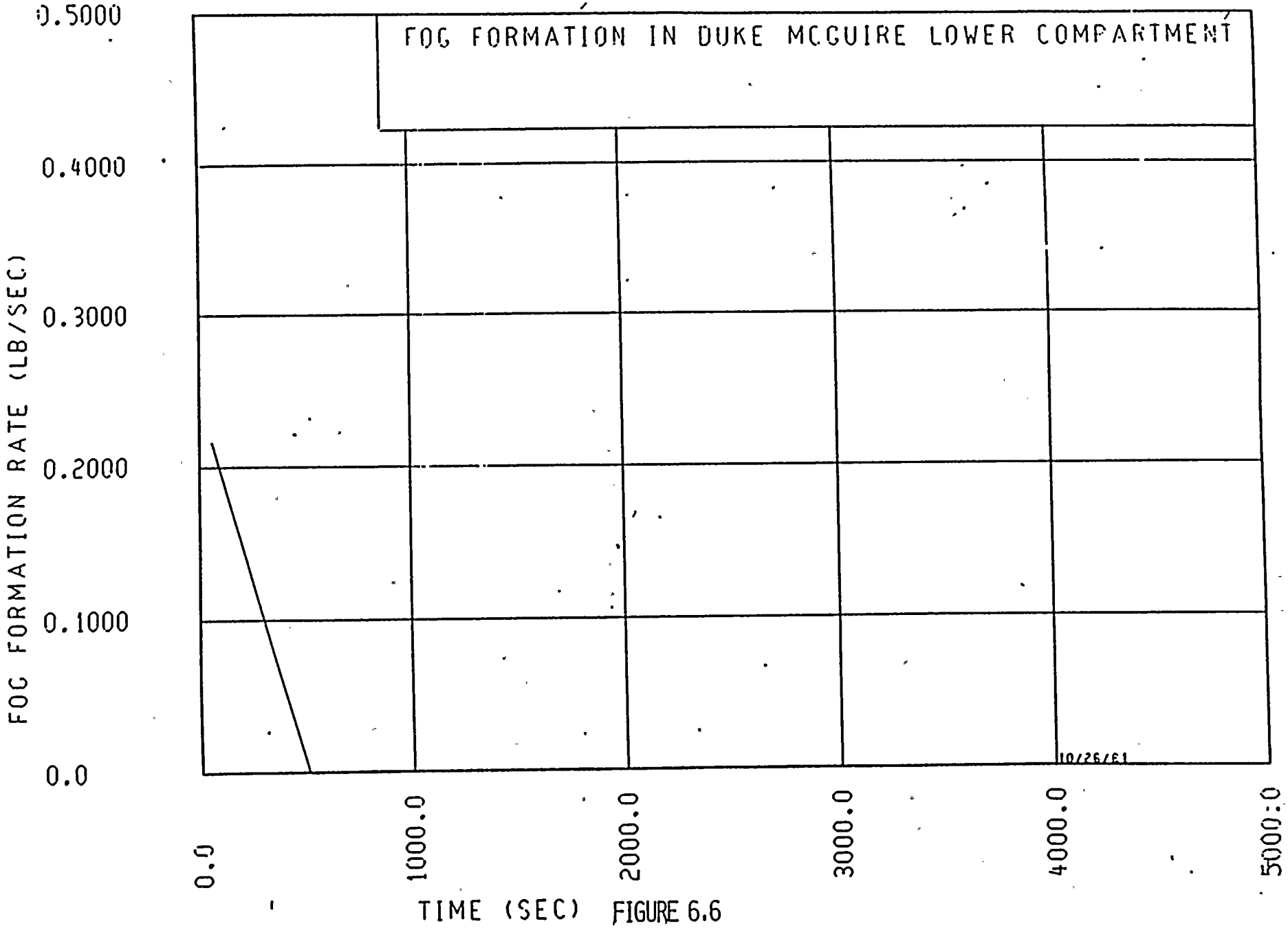
FOG FORMATION IN DUKE MCGUIRE LOWER COMPARTMENT
0.5000
0.4000
0.3000
0.2000
0.1000
0.0
FOG FORMATION RATE (LB/SEC)
0.0
1000.0
2000.0
3000.0
4000.0
5000.0
TIME (SEC)
10/26/81

FIGURE 6.6

FIGURE 6.7

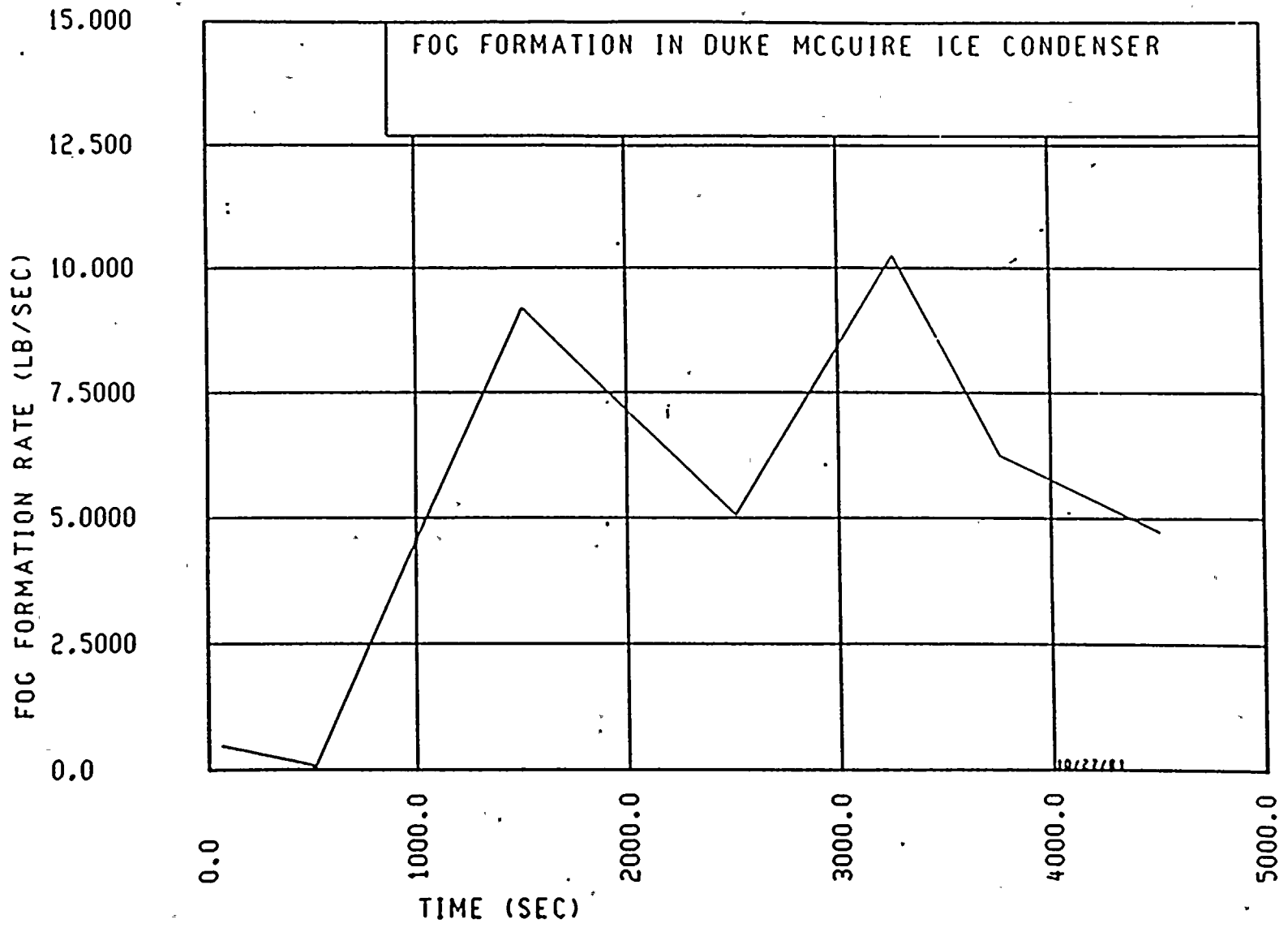
FOG FORMATION IN DUKE MCGUIRE ICE CONDENSER
FOG FORMATION RATE (LB/SEC)
15.000
12.500
10.000
7.5000
5.0000
2.5000
0.0
0.0
1000.0
2000.0
3000.0
4000.0
5000.0
TIME (SEC)

peak of 10.2 lb/sec at about 3260 seconds. The eight fog formation rates in the lower compartment and in the ice condenser are input to FOGMASS in a tabular form.

FOGMASS computes the rate of fog generation by the break flow, the fog settling rate due to gravity, and the fog removal rate due to sprays, as well as the rates of fog entrainment by intercompartmental and fan flows. The input data needed to calculate each of these rates are discussed as follows.

The rate of reactor coolant release to the containment and the coolant enthalpy were obtained from the MARCH output[7] for a small LOCA. The quality of the break flow was calculated using the enthalpy and the lower compartment gas temperature. According to the MARCH prediction[7] the discharge of liquid by the break flow into the lower compartment lasts for only 2172 seconds. Afterward, the water level in the reactor vessel drops below the break elevation and the fluid discharged from the break is essentially steam. Therefore, in the present study, it is assumed that no fog is generated by the break flow after 2172 seconds.

For fog removal by gravitational settling, a volume mean drop size of 10 μ was assumed. The assumption of 10 μ volume mean drop size is conservative, considering the fact that for a few thousand seconds the drop agglomeration mechanism would be able to increase volume mean drop size substantially. It should also be noted that a smaller volume mean drop size means that the minimum fog inerting concentration would be reduced and thus makes the present analysis conservative. Furthermore, no consideration was given to the deposition of fog on the walls and vertical surfaces of the structure, or for fog removal in the fan flows when it passes through ducts and fans. All the assumptions mentioned above make the present analysis very conservative. The containment geometric data needed in computing the settling rate are given in Table 6.8.

For fog removal by sprays, a spray flow rate of 6800 gpm was used for McGuire. According to the McGuire CLASIX analysis[28], the sprays are initiated at 124 seconds. A volume fraction of sprays (volume of sprays divided by volume of the spray zone) of 3.3×10^{-4} was used. As previously discussed a spray removal efficiency of a 100 percent efficiency was used.

In Figure 6.5, the directions of the intercompartmental flows are shown. The intercompartmental flow rates for the six flow paths and eight time steps were obtained from the OPS CLASIX analysis and are given in Table 6.9. The present analysis considers the intercompartmental flows as the mechanisms of transporting fog from one compartment to another. It was assumed in the present analysis that the fog concentrations in the intercompartment flows are the same as those in the compartments from which the flows are originated.

Figure 6.5 shows two trains of the air return fan and hydrogen skimmer system and the fan flow directions. The fans are initiated at 694 seconds. The fan head-flow curve reported in Reference 28 was used to compute the fan flow rates. Fan flow rates of 1000 ft^3/sec and 100 ft^3/sec were used for the air return fan and the hydrogen skimmer system, respectively. These flow rates were calculated using average Δp's between the upper compartment and the lower compartment, and between the dead ended region and the upper compartment. It was also assumed that the fog concentrations in the fan flows are the same as those in the compartments from which the flows are originated.

The results of the FOGMASS calculation are shown in Figure 6.8. It is seen that for the first few hundred seconds the fog concentrations in the lower compartment, ice condenser lower and upper plenums are about the same and increasing. At about 600 seconds, the lower compartment fog concentration reaches its peak of 1.6×10^{-4}. Afterward, the intercompartmental flows transport more fog droplets out of the lower compartment than are generated by the break flow and condensation and, therefore, the lower compartment fog concentration decreases. However, the upper plenum fog concentration keeps rising until about 800 seconds,

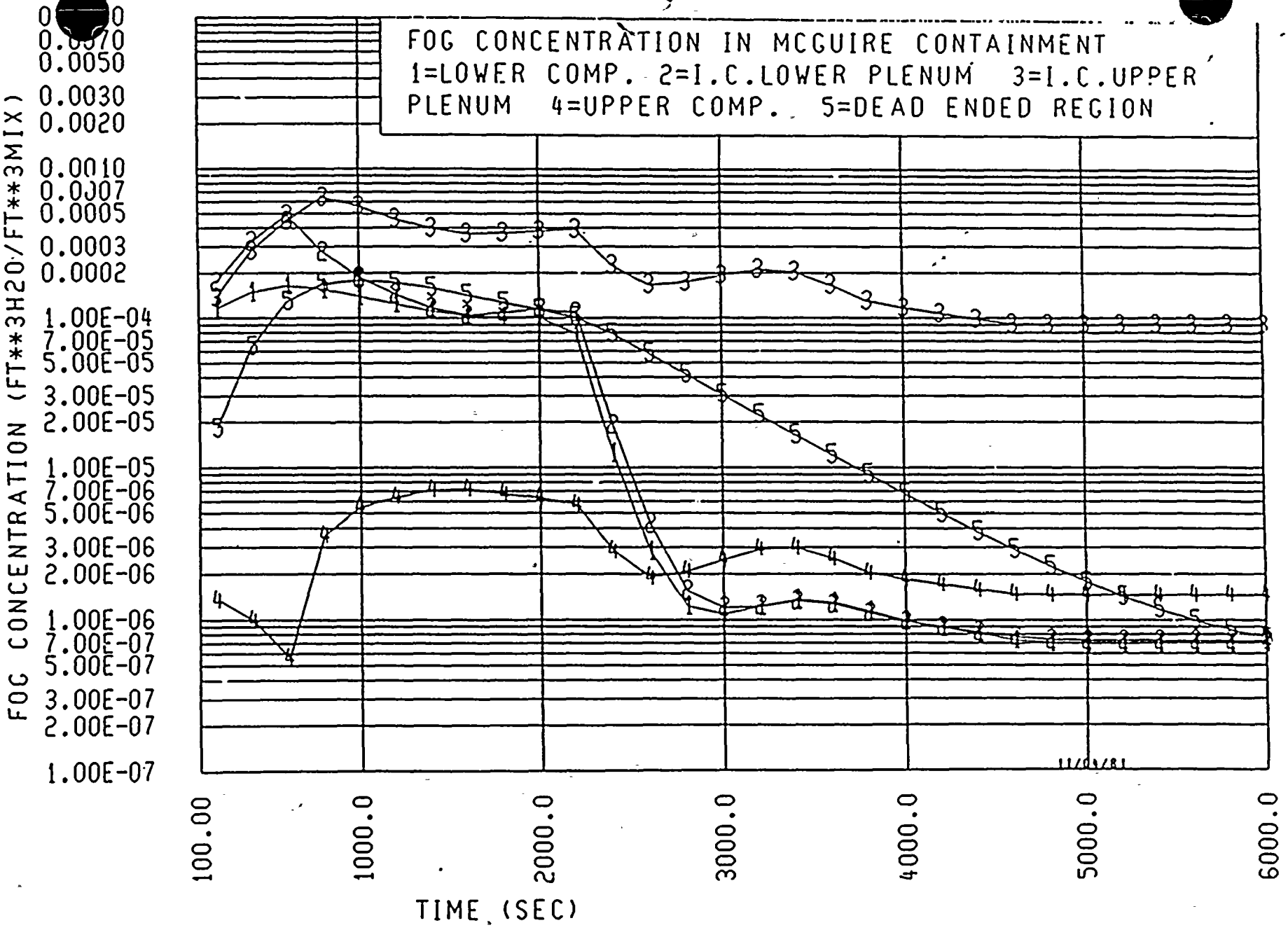
FOG CONCENTRATION IN MCGUIRE CONTAINMENT
1=LOWER COMP. 2=I.C.LOWER PLENUM 3=I.C.UPPER PLENUM 4=UPPER COMP. 5=DEAD ENDED REGION
FOG CONCENTRATION (FT**3H2O/FT**3MIX)
0.0070
0.0050
0.0030
0.0020
0.0010
0.0007
0.0005
0.0003
0.0002
1.00E-04
7.00E-05
5.00E-05
3.00E-05
2.00E-05
1.00E-05
7.00E-06
5.00E-06
3.00E-06
2.00E-06
1.00E-06
7.00E-07
5.00E-07
3.00E-07
2.00E-07
1.00E-07
100.00
1000.0
2000.0
3000.0
4000.0
5000.0
6000.0
TIME (SEC)

FIGURE 6.8

due to an increasing fog formation in the ice condenser and more fog entrained in the intercompartmental flow into the upper plenum. The upper plenum fog concentration reaches its peak of 6.4×10^{-4} at about 800 seconds. The lower plenum fog concentration is almost the same as the lower copartment fog concentration because of little difference in the intercompartmental flow rates into and out of the ice condenser lower plenum. Therefore, these two volumes behave as a single volume in terms of fog concentration.

At 2172 seconds, the break flow in the lower compartment stops generating fog and, therefore, the fog concentrations drop sharply thereafter. The effect is more pronounced for the lower compartment and lower plenum fog concentrations. The highest fog concentration exists in the ice condenser upper plenum while the lowest exists in the upper compartment. The effect of sprays on the upper compartment fog concentration is clearly seen in Figure 6.8. At 124 seconds, the sprays are turned on and the upper compartment fog concentration drops sharply until about 600 seconds. At about 600 seconds, the upper compartment fog concentration starts to increase again because the intercompartmental flow into the compartment increases sharply at that time. A peak concentration of 7.5×10^{-6} in the upper compartment is reached at about 1500 seconds.

Hydrogen starts to release into the containment at about 3804 seconds, according to the MARCH calculation[28]. It reaches 4 volume percent at about 4300, 4400, and 4850 seconds in the lower compartment, upper plenum, and upper compartment, respectively.

At 4300 seconds, the calculated lower compartment fog concentration is 8.4×10^{-7}, which is about an order of magnitude smaller than the minimum fog concentrations required for inerting 4 percent H_2. At 4850 seconds, the upper compartment fog concentration is 1.47×10^{-6}, which is about a factor of five smaller than the minimum fog concentration required for inerting 4 percent H_2*. At the times of

* The fog inerting criterion used is described in Section 5.2.

reaching 8.5 percent H_2, the fog concentrations in the lower and upper compartments are even lower than the figures given above. Therefore, it is concluded that the fog concentrations in the lower and upper compartments are too low to have any inerting effect. The use of the present theory on fog inerting also leads to the same conclusion.

However, at 4400 seconds, the calculated fog concentration in the upper plenum is 9.8×10^{-5} which is higher than the Factory Mutual fog inerting data extrapolated to 10 μ drops and the present theoretical prediction. The data shows that in order to inert 4.76 percent H_2 the fog concentration must be 8.4×10^{-6} or higher for 10 μ volume mean drop size. At 4500 seconds, the upper plenum hydrogen concentration reaches about 7 percent and the fog concentration is 9.3×10^{-5}. Again, an extrapolation of the Factory Mutual data to 10 μ shows that fog concentration of 2.1×10^{-5} or higher is required to inert 7.2 percent H_2. In comparison, the present theory on fog inerting predicts 1.02×10^{-4} for 7.2 percent H_2. Therefore, it appears that it is possible to inert 7 percent H_2, but unlikely. However, at 8 percent H_2 in the upper plenum, which occurs at about 4600 seconds, the fog concentration is 9.1×10^{-5}, which is too low to inert 8 percent H_2. An extrapolation of the Factory Mutual 8 percent H_2 data to 10 μ volume mean drop size and the present prediction give 1.9×10^{-4} and 1.2×10^{-4} for the minimum required fog inerting concentration, respectively. Therefore, both the theory and the extrapolation of the test data indicate that fog inerting will not occur.

The glow plug igniters which have been installed in the McGuire containment were designed to burn hydrogen lower than 8.5 percent. As discussed previously, no fog inerting effects will be expected in the McGuire lower and upper compartments. Therefore, the glow plug igniters are expected to function as designed in these two compartments. It may be possible that fog present in the ice condenser upper plenum may prevent the glow plug igniters from igniting hydrogen below 7 percent. However, it seems very unlikely that the same igniters would fail to ignite 8.5

*The fog inerting criterion used is described Section 5.2.

percent H_2 as designed, considering the fact that considerable conservatism has been exercised in the present analysis.

TABLE 6.6 FOG INPUT DATA FOR McGUIRE LOWER COMPARTMENT

Time (sec)	Lower Compartment Gas Flow Rate (ft^3/sec)	Gas Temp. (°F)	Wall Temp. (°F)	Total Pressure (psia)	Steam Partial Pressure (psia)
60	1624.6	160	149	16.5	7
510	1248.1	225	215	22.2	18.3
1510	2387.8	205	198	21.9	12.6
2010	2393.8	205	198	22	12.4
2510	1940.7	195	193	21.5	10.4
3260	2055.5	200	195	21.6	10.8
3760	1801.7	200	194	21	9.3
4510	1919.3	250	222	21.2	7.3

TABLE 6.7 FOG INPUT DATA FOR McGUIRE ICE CONDENSER

Time (sec)	Ice Condenser Gas Flow Rate (ft^3/sec)	Gas Temp. (°F)	Ice Temp. (°F)	Total Pressure (psia)	Steam Partial Pressure (psia)
60	820.5	90	32	16.5	1
510	107.1	130	32	22.2	2.3
1510	1926	190	32	21.9	9.3
2010	1637	193	32	22	9
2510	1145	188	32	21.4	8.6
3260	1630	195	32	21.6	10.3
3760	1514	193	32	21.1	8.1
4510	1464	192	32	22.1	7.1

TABLE 6.8 GEOMETRIC DATA FOR McGUIRE CONTAINMENT

	Volume (ft^3)	Floor Area (ft^2)
Lower Compartment	237,400	5,410
Ice Condenser Lower Plenum	24,200	3,100
Ice Condenser Upper Plenum	47,000	3,200
Upper Compartment	670,000	10,390
Dead Ended Region	130,900	3,350

TABLE 6.9 INTERCOMPARTMENTAL FLOW RATES (ft^3/sec)
PREDICTED BY CLASIX FOR McGUIRE

Time (sec)	Flow From LC to LP	Flow From LP to UP	Flow From UP to UC	Flow From UC to LC	Flow From DE to LC
6.001E1	1.351E3	8.205E2	5.783E2	-1.198E2	-1.538E2
5.100E2	8.716E2	1.071E2	-2.269E1	-2.863E1	-3.479E2
1.510E3	2.008E3	1.926E3	8.635E2	-1.900E2	-1.898E2
2.010E3	2.010E3	1.637E3	6.869E2	-2.266E2	-1.572E2
2.510E3	1.722E3	1.145E3	4.807E2	-1.410E2	-7.767E1
3.260E3	1.713E3	1.630E3	6.666E2	-2.087E2	-1.338E2
3.760E3	1.546E3	1.514E3	7.231E2	-1.289E2	-1.268E2
4.510E3	1.634E3	1.464E3	7.640E2	-1.328E2	-1.515E2

6.4 FOG INERTING PROBABILITY IN THE D. C. COOK PLANT

The computer codes, FOG and FOGMASS, were used to perform fog inerting analysis for the D. C. Cook plant. FOG was used to calculate the rates of fog formation due to boundary layer and bulk stream condensation in the D. C. Cook ice condenser and lower plenum. Then these fog formation rates were used in FOGMASS to compute the fog concentrations in each of the D. C. Cook containment subcompartments.

To compute the fog formation rates in the ice condenser upper plenum and lower compartment, some output data from the Cook CLASIX analysis[29] are needed. These data include time histories of gas temperature, wall temperature, total pressure, and steam partial pressure in each containment subcompartment, as well as the intercompartmental and fan flow rates. In order to utilize the CLASIX output data, the ice condenser containment is subcompartmentalized in the FOGMASS program in exactly the same manner as in Reference 29. The subcompartmentalization model used in the Cook CLASIX analysis is shown in Figure 6.9. In this study only the S_2D accident scenario has been analyzed.

The FOG input data for Cook S_2D Case 1 are given in Tables 6.10 and 6.11, and the calculational results are shown in Figures 6.10 and 6.11. In Figure 6.10, the fog formation rate in the lower compartment is shown. It is seen that the fog formation rate is negligibly small. It should be noted that the calculation of the lower compartment fog concentration in the D. C. Cook plant starts at 600 seconds instead of 60 seconds used for the other two plants. The fog formation rate in the lower compartment starts to increase at about 4200 seconds because of the increase in the steam partial pressure. It reaches 0.017 lb/sec at about 4590 seconds. Fog formation in the lower compartment will stop after 4700 seconds because of the hydrogen burn thereafter. The fog formation rate in the ice condenser is shown in Figure 6.11. It is seen that the fog formation rate in the ice condenser is much larger than that in the lower compartment. It increases with the ice condenser steam flow rate and reaches a peak of about 15.6 lb/sec at about 1200 seconds. The fog formation rate in the ice condenser then begins to decrease and is low at the time of significant hydrogen release.

FIGURE 6.9
D.C. COOK CLASIX MODEL

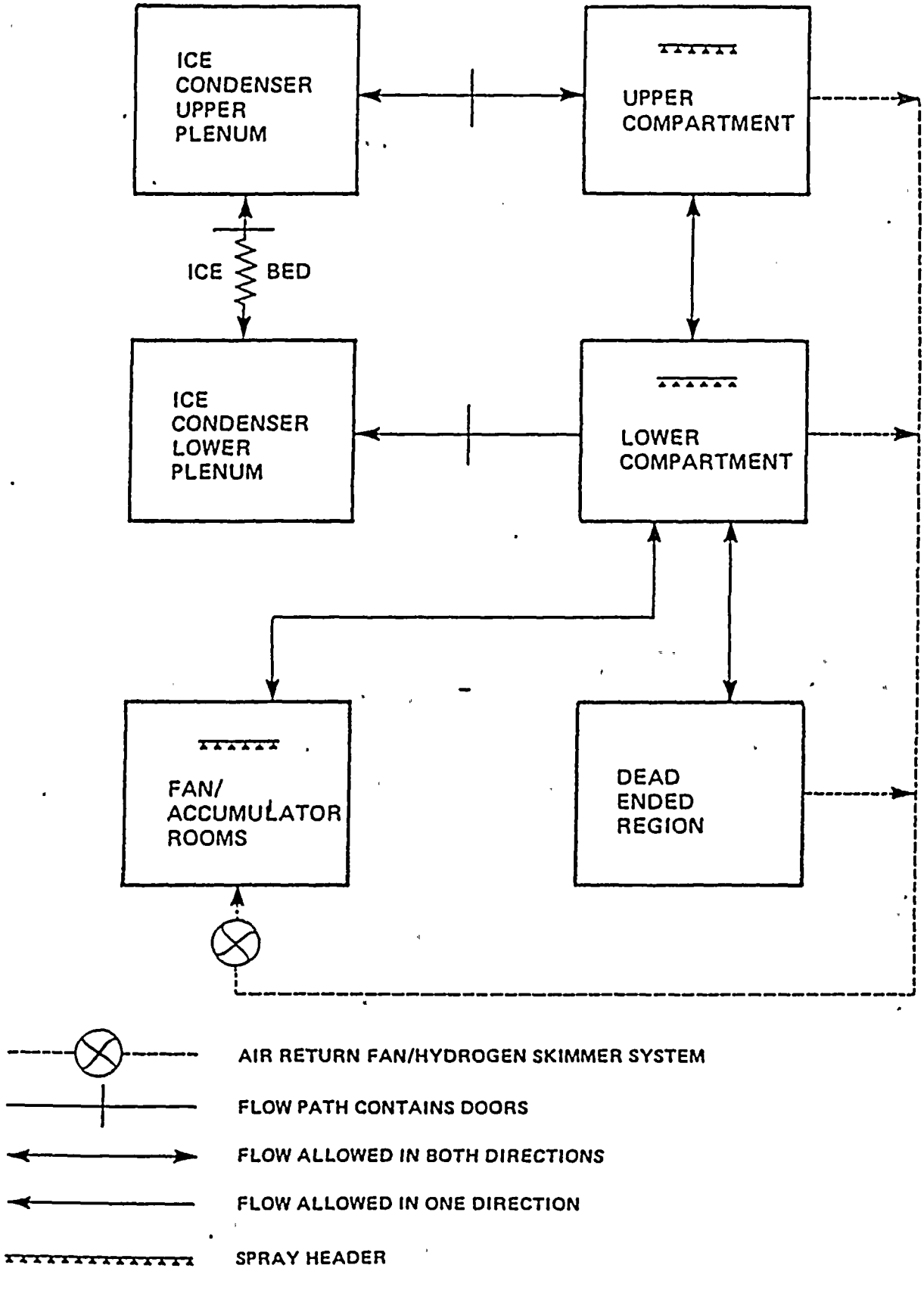

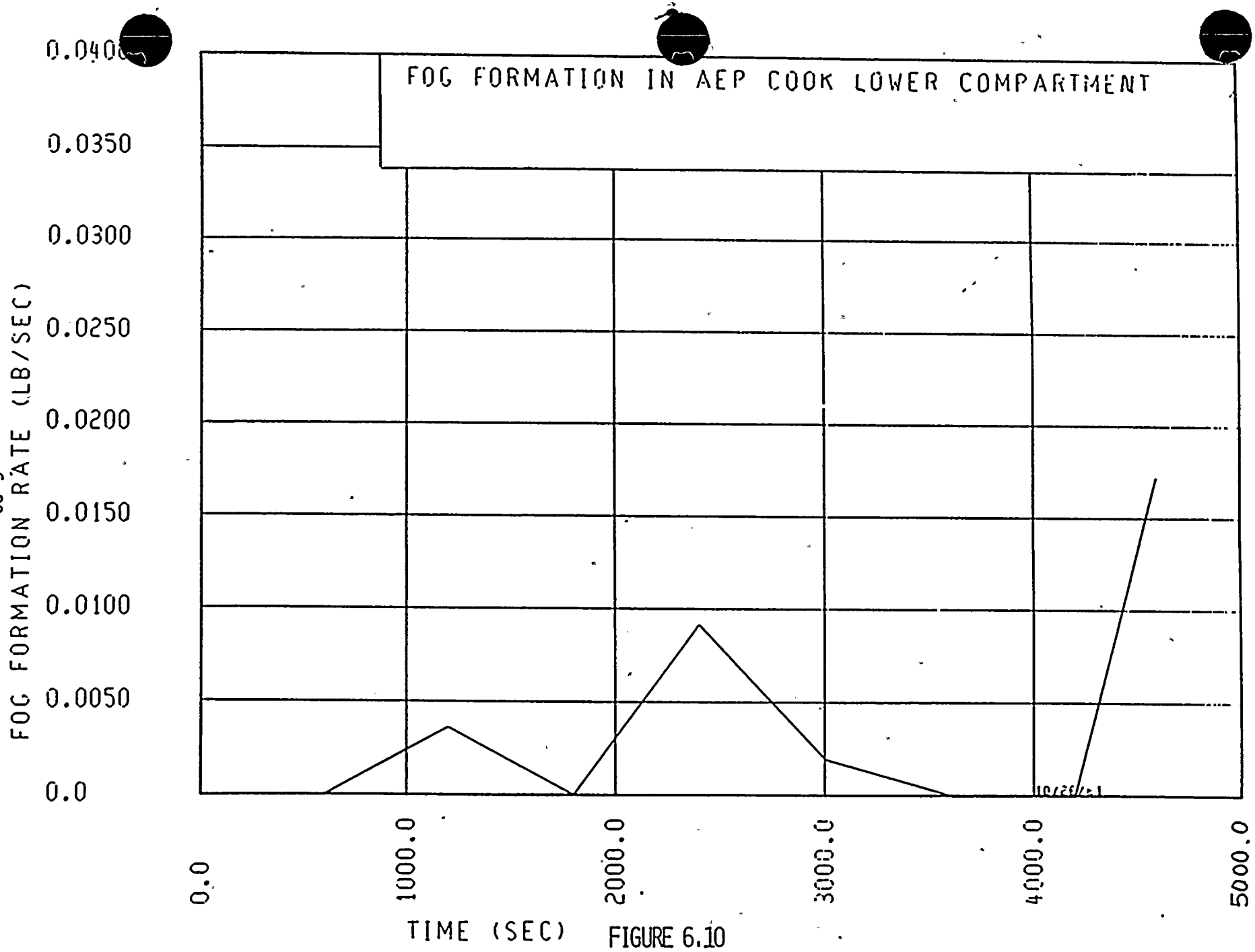
FOG FORMATION IN AEP COOK LOWER COMPARTMENT
0.0400
0.0350
0.0300
0.0250
0.0200
0.0150
0.0100
0.0050
0.0
FOG FORMATION RATE (LB/SEC)
6E-9
0.0
1000.0
2000.0
3000.0
4000.0
5000.0
TIME (SEC)

FIGURE 6.10

FIGURE 6.11

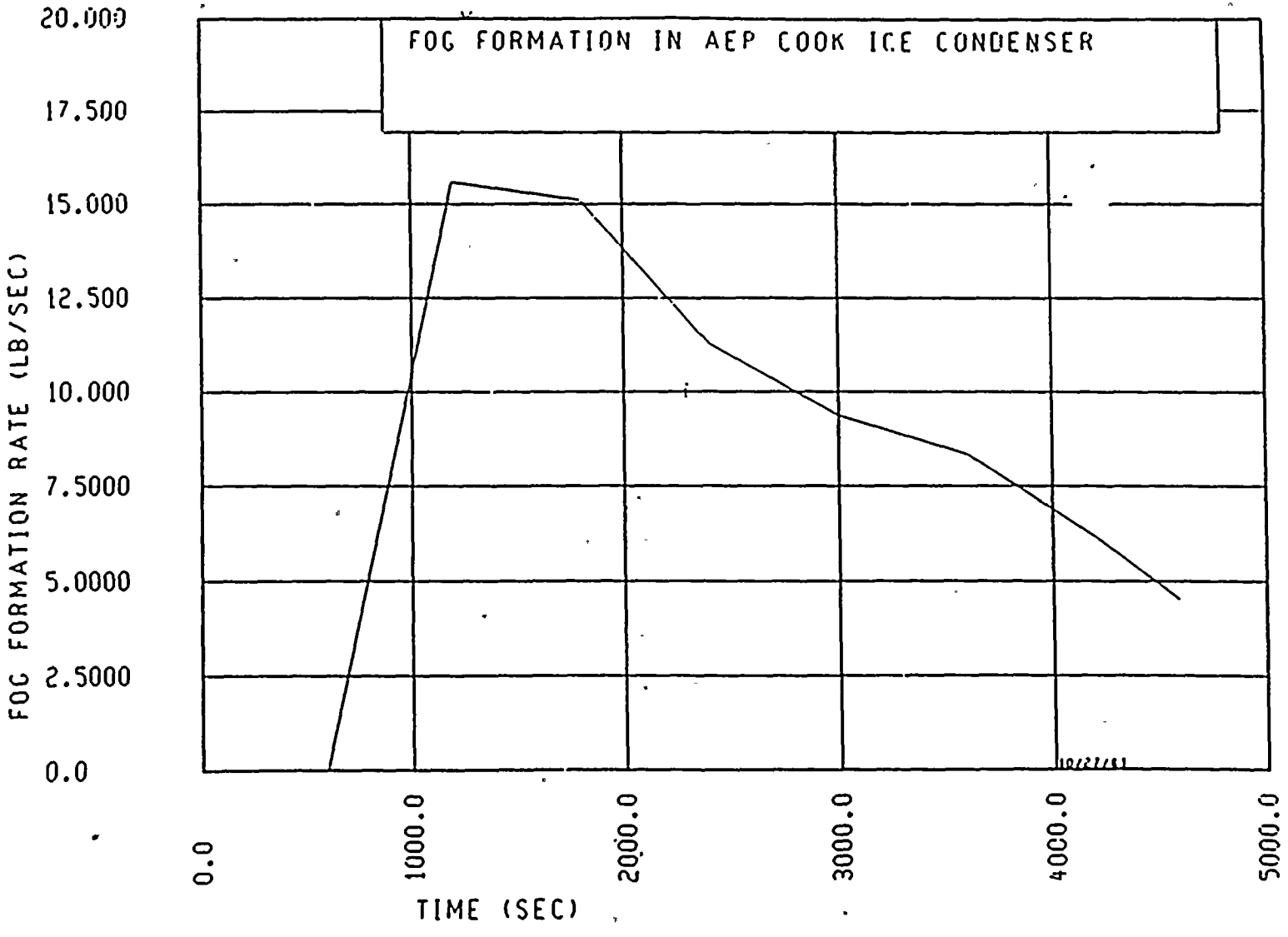
FOG FORMATION IN AEP COOK ICE CONDENSER
FOG FORMATION RATE (LB/SEC)
20.000
17.500
15.000
12.500
10.000
7.5000
5.0000
2.5000
0.0
0.0
1000.0
2000.0
3000.0
4000.0
5000.0
TIME (SEC)

The eight fog formation rates in the lower compartment and in the ice condenser are input to FOGMASS in a tabular form.

FOGMASS computes the rate of fog generation by the break flow, the fog settling rate due to gravity, and the fog-removal rate due to sprays, as well as the rates of fog entrainment by intercompartmental and fan flows. The input data needed to calculate each of these rates are discussed as follows.

The rate of reactor coolant release to the containment and the coolant enthalpy were obtained from the MARCH output[7] for a small LOCA. The quality of the break flow was calculated using the enthalpy and the lower compartment gas temperature. According to the MARCH prediction[7] the discharge of liquid by the break flow into the lower compartment lasts for only 2172 seconds. Afterward, the water level in the reactor vessel drops below the break elevation and the fluid discharged from the break is essentially steam. Therefore, in the present study, it is assumed that no fog is generated by the break flow after 2172 seconds.

For fog removal by gravitational settling, a volume mean drop size of 10 μ was assumed. The assumption of 10 μ volume mean drop size is conservative, considering the fact that for a few thousand seconds the drop agglomeration mechanism would be able to increase volume mean drop size substantially. It should also be noted that a smaller volume mean drop size means that the minimum fog inerting concentration would be reduced and thus makes the present analysis even more conservative. Furthermore, no consideration was given to the deposition of fog on the walls and vertical surfaces of the structure, or for fog removal in the fan flows when it passes through ducts and fans. All the assumptions mentioned above make the present analysis very conservative. The containment geometric data needed in computing the settling rate are given in Table 6.12.

For fog removal by sprays, spray flow rates of 4000, 1800, and 528 gpm were used for the upper compartment, lower compartment, and fan/accumulator rooms, respectively. According to the Cook CLASIX analysis[29], the sprays are initiated at 141 seconds. A volume fraction of sprays (volume of sprays divided by volume of the spray zone) of 3.3×10^{-4} was used. As previously discussed a spray removal efficiency of a 100 percent efficiency was used.

In Figure 6.9, the directions of the intercompartmental flows are shown. The intercompartmental flow rates for the six flow paths and eight time steps were obtained from the OPS CLASIX analysis and are given in Table 6.13. The present analysis considers the intercompartmental flows as the mechanisms of transporting fog from one compartment to another. It was assumed in the present analysis that the fog concentrations in the intercompartment flows are the same as those in the compartments from which the flows are originated.

Figure 6.9 shows two trains of the air return fan and hydrogen skimmer system and the fan flow directions. The fans are initiated at 711 seconds. The fan head-flow curve reported in Reference 29 was used to compute the fan flow rates. Fan flow rates of 1388, 61.76, and 4.13 ft^3/sec were used for the flows from the upper compartment, lower compartment, and dead ended region to the fan/accumulator rooms, respectively. These flow rates were calculated using the Δp's between the the fan/accumulator rooms and three other compartments. It was also assumed that the fog concentrations in the fan flows are the same as those in the compartments from which the flows are originated.

The results of the FOGMASS calculation are shown in Figure 6.12. It is seen that for the first few hundred seconds the fog concentrations in the lower compartment, and the ice condenser lower plenum are high. At about 140 seconds, the lower compartment fog concentration reaches its peak of 1×10^{-4}. After the sprays are initiated at 141 seconds, the fog concentrations in the lower compartment, upper compartment, and fan/accumulator rooms drop sharply. However, the upper plenum fog concentration keeps rising until about 1200 seconds, due to an increasing

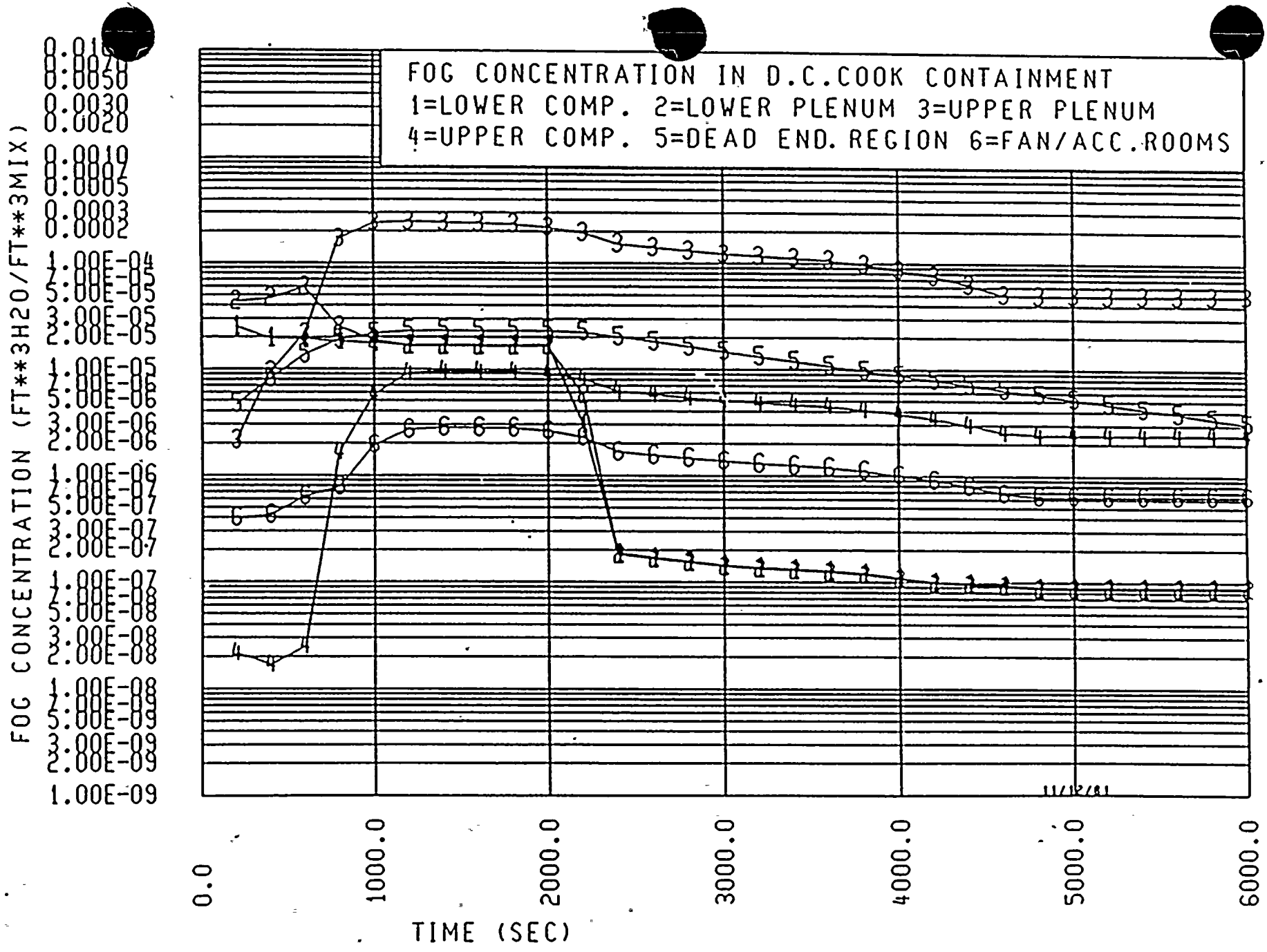
FOG CONCENTRATION IN D.C.COOK CONTAINMENT
1=LOWER COMP. 2=LOWER PLENUM 3=UPPER PLENUM
4=UPPER COMP. 5=DEAD END. REGION 6=FAN/ACC.ROOMS
FOG CONCENTRATION (FT**3H2O/FT**3MIX)
0.0050
0.0030
0.0020
0.0010
0.0007
0.0005
0.0003
0.0002
1.00E-04
2.00E-05
5.00E-05
3.00E-05
2.00E-05
1.00E-05
2.00E-06
5.00E-06
3.00E-06
2.00E-06
1.00E-06
2.00E-07
5.00E-07
3.00E-07
2.00E-07
1.00E-07
2.00E-08
5.00E-08
3.00E-08
2.00E-08
1.00E-08
2.00E-09
5.00E-09
3.00E-09
2.00E-09
1.00E-09
0.0
1000.0
2000.0
3000.0
4000.0
5000.0
6000.0
TIME (SEC)

FIGURE 6.12

fog formation in the ice condenser and more fog entrained in the intercompartmental flow into the upper plenum. The upper plenum fog concentration reaches its peak of 2.4×10^{-4} at about 1200 seconds. After about 1200 seconds, the lower plenum fog concentration is almost the same as the lower copartment fog concentration since the intercompartmental flows quickly make the fog concentrations in these two compartments uniform. Therefore, these two volumes behave as a single volume in terms of fog concentration.

At 2172 seconds, the break flow in the lower compartment stops generating fog and, therefore, the fog concentrations drop sharply thereafter. The effect is more pronounced for the lower compartment and lower plenum fog concentrations. The highest fog concentration exists in the ice condenser upper plenum. The effect of sprays on the upper compartment fog concentration is clearly seen in Figure 6.12. At 141 seconds, the sprays are turned on and the upper compartment fog concentration drops sharply until about 300 seconds. At about 300 seconds, the upper compartment fog concentration starts to increase again because the intercompartmental flow into the compartment increases sharply at that time. A peak concentration of 9.5×10^{-6} in the upper compartment is reached at about 1400 seconds.

Hydrogen starts to release into the containment at about 3804 seconds, according to the MARCH calculation[29]. It reaches 4 volume percent at about 4350, 4370, and 4700 seconds in the lower compartment, upper plenum, and upper compartment, respectively.

At 4350 seconds, the calculated lower compartment fog concentration is 10^{-7}, which is about two orders of magnitude smaller than the minimum fog concentrations required for inerting 4 percent H_2. At 4700 seconds, the upper compartment fog concentration is 2.4×10^{-6}, which is about a factor of two smaller than the minimum fog concentration required for inerting 4 percent H_2*. At the times of reaching 8.5

---

* The fog inerting criterion used is described in Section 5.2.

percent H_2, the fog concentrations in the lower and upper compartments are even lower than the figures given above. Therefore, it is concluded that the fog concentrations in the lower and upper compartments are too low to have any inerting effect. The use of the present theory on fog inerting also leads to the same conclusion.

However, at 4370 seconds, the calculated fog concentration in the upper plenum is 6.5×10^{-5} which is higher than the Factory Mutual fog inerting data extrapolated to 10 μ drops and the present theoretical prediction. The data shows that in order to inert 4.76 percent H_2 the fog concentration must be 8.4×10^{-6} or higher for 10 μ volume mean drop size. At 4530 seconds, the upper plenum hydrogen concentration reaches about 7 percent and the fog concentration is 5.5×10^{-5}. Again, an extrapolation of the Factory Mutual data to 10 μ shows that fog concentration of 2.1×10^{-5} or higher is required to inert 7.2 percent H_2. In comparison the present theory of fog inerting predicts 1.02×10^{-4} for 7.2 percent H_2. Therefore, it appears that it is possible to inert 7 percent H_2, but unlikely. However, at 8 percent H_2 in the upper plenum, which occurs at about 4600 seconds, the fog concentration is 5.1×10^{-5}, which is too low to inert 8 percent H_2. An extrapolation of the Factory Mutual 8 percent H_2 data to 10 μ volume mean drop size and the present prediction give 1.9×10^{-4} and 1.2×10^{-4} for the minimum required fog inerting concentration, respectively.

The glow plug igniters which have been installed in the Cook containment were designed to burn hydrogen lower than 8 percent. As discussed previously, no fog inerting effects will be expected in the Cook lower and upper compartments. Therefore, the glow plug igniters are expected to function as designed in these two compartments. It may be possible that fog present in the ice condenser upper plenum may prevent the glow plug igniters from igniting hydrogen below 7 percent. However, it seems very unlikely that the same igniters would fail to ignite 8 percent H_2 as designed, considering the fact that considerable conservatism has been exercised in the present analysis.

TABLE 6.10 FOG INPUT DATA FOR D. C. COOK LOWER COMPARTMENT

Time (sec)	Lower Compartment Gas Flow Rate (ft^3/sec)	Gas Temp. (°F)	Wall Temp. (°F)	Total Pressure (psia)	Steam Partial Pressure (psia)
600	799.4	222	215.2	21.8	17.4
1200	2798.2	190	183.5	20.2	9.4
1800	2805.8	190	180.3	20	9.1
2400	2513.6	180	177.2	19.6	7.6
3000	2448.5	178	170.4	19.3	7.2
3600	2359.7	175	169.3	19.2	6.4
4200	2272.3	165	161.9	18.8	5.3
4590	2482.7	168	161	19.5	5.8

TABLE 6.11 FOG INPUT DATA FOR D. C. COOK ICE CONDENSER

Time (sec)	Ice Condenser Gas Flow Rate (ft^3/sec)	Gas Temp. (°F)	Ice Temp. (°F)	Total Pressure (psia)	Steam Partial Pressure (psia)
600	76	147	32	21.8	3.4
1200	2548	190	32	20.1	9.3
1800	2572	188	32	19.9	9.0
2400	2359	184	32	19.7	7.9
3000	2256	187	32	19.3	7.1
3600	2199	175	32	19.2	6.6
4200	2126	166	32	18.8	5.3
4590	2312	163	32	19.8	4.3

TABLE 6.12 GEOMETRIC DATA FOR D. C. COOK CONTAINMENT

	Volume (ft^3)	Floor Area (ft^2)
Lower Compartment	249,681	5,410
Ice Condenser Lower Plenum	24,700	3,100
Ice Condenser Upper Plenum	47,010	3,200
Upper Compartment	681,283	10,390
Dead Ended Region	61,105	853
Fan/Accumulator Rooms	54,828	2,500

TABLE 6.13 INTERCOMPARTMENTAL FLOW RATES (ft^3/sec)
PREDICTED BY CLASIX FOR D. C. COOK

Time (sec)	Flow From LC to LP	Flow From LP to UP	Flow From UP to UC	Flow From UC to LC	Flow From DE to LC	Flow From F/A to LC
600	6.387E2	7.600E1	-4.410E1	-3.746E1	-1.232E2	-1.229E2
1200	2.577E3	2.548E3	1.106E3	-1.740E2	-4.720E1	1.509E3
1800	2.600E3	2.572E3	1.155E3	-1.620E2	-4.381E1	1.529E3
2400	2.356E3	2.359E3	1.145E3	-1.325E2	-2.512E1	1.595E3
3000	2.273E3	2.256E3	1.178E3	-1.463E2	-2.923E1	1.553E3
3600	2.202E3	2.199E3	1.190E3	-1.334E2	-2.333E1	1.603E3
4200	2.136E3	2.126E3	1.258E3	-1.183E2	-1.802E1	1.642E3
4590	2.346E3	2.312E3	1.400E3	-1.130E2	-2.371E1	1.650E3

6.5 EFFECT OF FOG ON GLOBAL COMBUSTION

In order to assess the effect of fog on the deflagration limit of hydrogen, which is defined as the minimum hydrogen concentration at which the flame propagates in all directions, a flame temperature criterion which considers fog droplets as a heat sink was used. This criterion assumes that the critical flame temperature of 710°C is still applicable to a hydrogen mixture which contains fog droplets. For a given fog concentration, the heat required to heat a unit mass of the mixture to 710°c can be calculated. Then the hydrogen concentration needed to supply this amount of heat, assuming 100 percent combustion, can be determined. Using this method, the calculated fog concentrations of 5.5×10^{-5} and 5.1×10^{-5} for the Sequoyah plant at 4650 seconds and for the D. C. Cook Plant at 4600 seconds, respectively, were found to be capable of raising the deflagration limit to 10.6 vol. percent H_2. In comparison, the calculated fog concentration of 9.1×10^{-5} for the McGuire plant at 4600 seconds was found to be capable of raising the deflagration limit to 12 vol. percent H_2. This study shows that in order to achieve global combustion in the upper plenum, hydrogen concentration higher than 8.5 percent may be required. The effect of increasing hydrogen concentration required to obtain global combustion in the upper plenum should be investigated.

7.0 SUMMARY AND CONCLUSIONS

The present study has developed a systematic methodology to study the potential fog inerting problem for the PWR ice condenser plants. In the present investigation, major fog formation and removal mechanisms are identified and quantified. Theoretical models are developed to predict the fog formation rate due to boundary layer and bulk stream condensation, the fog removal rates due to gravitational settling and containment sprays. The mass conservation equations for the fog droplets in each of the containment subcompertments are solved simultaneously in order to obtain time histories of fog concentration. These equations incorporate fog formation due to condensation, fog generation due to break flow, fog removal due to gravitational settling and sprays, transport of fog by the intercompartmental flows and fan flows. Computer programs FOG and FOGMASS have been developed to compute fog formation rates and fog concentrations in each of the containment subcompartments. These two computer programs have been used to analyze a S_2D accident sequence for the Sequoyah, McGuire, and D.C. Cook plants. The analyses employed output data from the Sequoyah CLASIX analyses. Specifically, time histories of gas temperature, wall temperature, total pressure, and steam partial pressure in each containment subcompartment, as well as the intercompartmental and fan flow rates were used in the present analysis.

A fog inerting criterion has been developed to predict the minimum fog concentration required to inert a given hydrogen concentration and volume mean fog drop size. The present fog inerting criterion has been shown to be in agreement with the Factory Mutual data. The criterion shows that the minimum fog inerting concentration varies with the square of the volume mean fog drop size.

The present study shows that the fog concentrations in the upper and lower compartments of the three plants analyzed are too low to have any inerting effect on hydrogen mixtures. Therefore, the proposed glow plug igniters are expected to function as designed in these two compartments. It may be possible that fog present in the ice condenser upper

plenum may prevent the glow plug igniters from igniting hydrogen below 7 percent. However, it seems very unlikely that the same igniters would fail to ignite 8.5 percent H_2 as designed.

It should be recognized that the existing theories and data can only predict the minimum fog concentration for inerting. Further work may be required to verify the fog inerting theory associated with flame propagation in all directions.

ACKNOWLEDGMENTS

The author wishes to express his sincere gratitude to Mr. N.J. Liparulo, Drs. V. Srinivas, B. Lewis, and B. Karlovitz for assistance, suggestions, and helpful discussions, particularly in the area of the fog inerting criteria and the flame temperature criteria for fog, to Messrs. D. F. Paddleford, R. Bryan, F. G. Hudson, and K. Shiu for valuable comments, to Mr. K. C. Perry, Mr. S. J. Reiser, and Ms. R. M. Mariner for providing data on the three ice condenser plants, and to Mr. T. J. Miele for providing programming assistance.

He also would like to thank TVA, Duke Power, and AEP for providing the financial support.

REFERENCES

1. B. Lowry, "Preliminary Results: A Study of Hydrogen Igniters," ENN80-45, Lawrence Livermore National Laboratory, November 17, 1980.

2. "Additional Questions on Hydrogen Control System for Ice Condenser Plants," NRC memo from L. Rubenstein to R. Tedesco, dated June 26, 1981.

3. "The Marvikken Full Scale Containment Experiments," MXB-301 AB Atomenergi, March, 1977.

4. T. F. Kanzleiter, "LOCA Experiments With a PWR Multi-Compartment Model Containment," Trans. 1977 LWR Safety Conf., Idaho Falls, Idaho, 1977.

5. G. M. Fuls, "The CLASIX Computer Program for the Hydrogen Release and Degradation", OPS-07A35, Offshore Power Systems, 1981.

6. K. K. Almenas, "The Physical State of Post-Loss-of-Coolant Accident Containment Atmospheres," Vol. 44, Nuclear Technology, pp. 411-427, August, 1979.

7. "Summary of Analysis of Ice Condenser Containment Response to Hydrogen Transients," Offshore Power Systems report No. RP-28A52, September, 1980.

8. R. Brown and J. L. York, "Sprays Formed by Flashing Liquid Jets," Vol. 8, No. 2, AICh.E Journal, p. 149, May, 1962.

9. R. G. Gido, and A. Koestel, "LOCA-Generated Drop Size Prediction - A Thermal Framentation Model," Trans. Am. Nucl. Soc., 30, p. 371, 1978.

10. P. G. Hill, H. Witting, and E. P. Demetri, "Condensation of Metal Vapors During Rapid Expansion," Journal of Heat Transfer, p. 303, November, 1963.

11. M. Volmer and H. Flood, Z. Physik Chemie, A170, p. 273, 1934.

12. C. E. Junge, Advan. Geophys., H. Landsberg and J. Van Mieghem, ed., 4.1, Academic Press, New York, 1958.

13. R. J. Burian, and P. Cybulskis, "CORRAL II User Manual," Battelle Columbus Laboratories, January, 1977.

14. R. K. Hilliard and L. F. Coleman, "Natural Transport Effects on Fission Product Behavior in the Containment Systems Experiment," BNWL-7457, Battelle-Northwest, Richland, Washington, 1970.

15. N. H. Fletcher, J. Chem. Phys., 29, p. 572; 31, p. 1136, 1958.

16. D. E. Rosner and M. Epstein, "Fog Formation Conditions Near Cold Surfaces," Vol. 28, No. 1, J. of Colloid and Interface Sci., September, 1968.

17. K. Hijikata, and Y. Mori, "Forced Convective Heat Transfer of a Gas With Condensing Vapor Around a Flat Plate," Vol. 2, No. 1, Heat Transfer - Jap. Res., pp. 81-101, January, 1973.

18. M. Neiburger and C. W. Chien, "Computation of the Growth of Cloud Drops by Condensation Using an Electronic Digital Computer," Geophys. Monograph No. 5, pp. 191-209, 1960.

19. R. M. Kemper, "Iodine Removal by Spray in the Salem Station Containment," WCAP-7952, Westinghouse Electric Corp., August, 1972.

20. N. J. Liparulo, J. E. Olhoeft and D. F. Paddleford, "Glow Plug Ignitor Tests in H_2 Mixtures," WCAP-5909, Westinghouse Electric Corp., March 6, 1981.

21. R. G. Zalosh and S. N. Bajpai, "Water Fog Inerting of Hydrogen - Air Mixtures," EPRI Project Preliminary Rp. 1932-1, September, 1981.

22. J. M. Marchello, "Control of Air Pollution Source," Marcel Dekker, Inc., New York, 1976.

23. Letter from B. Lewis and B. Karlovitz to L. E. Hochreiter, dated may 5, 1980.

24. M. Berman, et al., "Analysis of Hydrogen Mitigation for Degraded Core Accidents in the Sequoyah Nuclear Power Plant," Sandia draft report, December 1, 1980.

25. T. von Karman, Unpublished notes, 1956.

26. S. S. Tsai, "Flame Temperature Criteria Tests," NS-CCA-81-039, Westinghouse internal memo, dated June 17, 1981.

27. Attachment to Offshore Power System letter PST-NE-109, dated May 22, 1981.

28. Attachment to Offshore Power System letter PST-NE-106, dated May 14, 1981.

29. Attachment to Offshore Power System letter PST-NE-218, dated August 6, 1981.

30. M. L. Corrin, J. R. Connel, and A. J. Gero, "An Assessment of Warm Fog - Nucleation, Control, and Recommended Research," NASACR-2477, November, 1974.

APPENDIX A

COMPUTATION OF Y_o AND ξ IN EQUATION (3.12)

The Hijikata-Mori fog formation theory[17] used the boundary layer approximation for the continuity, momentum, and energy equations. The fog concentration and velocity profiles in the boundary layer are assumed in Eqs. (3.7) and (3.8). Substituting Eqs. (3.7) through (3.10) into the conservation equations, we have

$$-\frac{3}{16}+\frac{3}{16}\xi+\frac{7}{120}Y_o+v'_\infty=0 \tag{A-1}$$

$$-(1+Y_o)\frac{V_o}{R}-\frac{3}{16}+\frac{3}{16}\xi+\frac{7}{120}V+\frac{1}{20}\xi V_\infty+v'_\infty=0 \tag{A-2}$$

$$-\frac{9}{35}+\frac{9}{35}\xi+\frac{311}{10080}Y_o+v'_\infty=-\frac{3}{2}(1+\xi)\frac{1}{R} \tag{A-3}$$

$$A(n)+B(n)\xi+\left\{C(n)+\frac{7}{120}E\right\}Y_o=\frac{1}{R}\left\{\frac{n}{Pr}-V_o-V_o(1+E)Y_o\right\} \tag{A-4}$$

where $A(n)=\dfrac{3(n+5)}{4(n+1)(n+3)(n+4)}$

$B(n)=\dfrac{3(n+6)}{4(n+2)(n+3)(n+4)}$

$C(n)=\dfrac{3(n+7)}{4(n+3)(n+5)(n+6)}$

$V_\infty=\dfrac{\Delta W}{1-W_\infty}$

$V_o=\dfrac{2\Delta W}{(1-W_o)S_c}$

$E=\dfrac{h_{fg}}{C_{pg}\Delta T}$

$$R = \frac{a^2 U_\infty}{\nu}$$

$$v'_\infty = \frac{\delta v_\infty}{a U_\infty}$$

W_∞ = weight fraction of vapor at free stream
W_0 = weight fraction of vapor at wall
ΔW = $W_\infty - W_0$
S_c = Schmidt number
ν = kinetic viscosity
v_∞ = component of the free stream velocity perpendicular to the wall
h_{fg} = heat of vaporization
C_{pg} = specific heat of non-condensible gas
ΔT = $T_\infty - T_0$
T_∞ = gas temperature at free stream
T_0 = gas temperature at wall

Equations (A-1) through (A-4) are four algebraic equations for four unknowns, Y_0, ξ, R, and v'_∞. These equations have been solved by the computer program FOG. In FOG, the values of Y_0, ξ, and R are computed and used in Eq. (3.12) to compute the fog formation rate.

APPENDIX B

DERIVATION OF EQUATION (5.5)

This appendix gives detailed procedures to derive Eq. (5.5), starting from Eq. (5.4)

$$(K)_{crit}\,\theta_i = f\left((Y_u - Y_f)/\theta_i\right) \tag{5.4}$$

where the ratio of heat loss rate per unit volume to the heat release rate by chemical reaction per unit volume, $(K)_{crit}$, is defined as

$$K_{crit} = S/C_p w \tag{B-1}$$

and the ratio of sensible heat to heat of combustion, θ_i, is defined as

$$\theta_i = C_p\,(T_i - T_u)/q \tag{B-2}$$

To arrive at Eq. (5.5), it is necesary to assume that all the heat loss is attributed to convection heat transfer to fog droplets of only one drop size. Under this assumption, the rate of heat loss per unit volume per degree, S, may be expressed as

$$S = n\pi d^2 h$$

where n = number of drops per unit volume
d = volume mean drop size
h = heat transfer coefficient

It is further assumed that the relative velocity between the droplets and the mixture flow is so small that heat transfer coefficient, h, can be approximated by the conduction limit. Under this assumption, Eq. (B-3) reduces to

$$S = \frac{12n\bar{\lambda}}{d^2} \tag{B-4}$$

ATTACHMENT 5 TO AEP:NRC:0500K
FOG INERTING CRITERIA FOR HYDROGEN/AIR MIXTURES
DONALD C. COOK NUCLEAR PLANT UNIT NOS. 1 AND 2